LBL-14008
Preprint

Lawrence Berkeley Laboratory

UNIVERSITY OF CALIFORNIA

RECEIVED
LAWRENCE
BERKELEY LABORATORY
MAR 29 1982
LIBRARY AND
DOCUMENTS SECTION

ENERGY & ENVIRONMENT DIVISION

To be submitted to Combustion Science and Technology

RADIATIVE EFFECTS ON DIFFUSION FLAME HEIGHTS

C.L. Cagle and P.J. Pagni

January 1982

TWO-WEEK LOAN COPY

This is a Library Circulating Copy which may be borrowed for two weeks. For a personal retention copy, call Tech. Info. Division, Ext. 6782

Prepared for the U.S. Department of Energy under Contract W-7405-ENG-48

LBL-14008 c.2

DISCLAIMER

This document was prepared as an account of work sponsored by the United States Government. While this document is believed to contain correct information, neither the United States Government nor any agency thereof, nor the Regents of the University of California, nor any of their employees, makes any warranty, express or implied, or assumes any legal responsibility for the accuracy, completeness, or usefulness of any information, apparatus, product, or process disclosed, or represents that its use would not infringe privately owned rights. Reference herein to any specific commercial product, process, or service by its trade name, trademark, manufacturer, or otherwise, does not necessarily constitute or imply its endorsement, recommendation, or favoring by the United States Government or any agency thereof, or the Regents of the University of California. The views and opinions of authors expressed herein do not necessarily state or reflect those of the United States Government or any agency thereof or the Regents of the University of California.

RADIATIVE EFFECTS ON

DIFFUSION FLAME HEIGHTS

C. L. Cagle* and P. J. Pagni
Energy and Environment Division
Lawrence Berkeley Laboratory and
Mechanical Engineering Department
University of California
Berkeley, CA 94720

* Submitted in partial fulfillment of the requirements for the degree of Master of Science in Mechanical Engineering, December 1981.

This work was supported by the Center for Fire Research in the U.S.D.O.C. National Bureau of Standards under Grant No. NB 80 NAG-E6839 which was administered by the U.S. Department of Energy under Contract No. W-7405-ENG-48 at the Lawrence Berkeley Laboratory, University of California.

ABSTRACT

A theoretical study of the effects of radiation in a combusting boundary layer over an inert extension of the pyrolyzing surface is presented for the free flow case. The calculation of the radiant energy flux at the surface is simplified by an optically thin approximation. Prandtl and Lewis numbers are assumed constant, and seven dimensionless parameters describe the system. Including radiation in the model increases the predicted flame lengths for liquid fuels and decreases the predicted flame lengths for solid fuels. The effects of varying each of the seven parameters individually are predicted. An approximate expression for the radiative flame height of a solid fuel in free flow is determined.

CONTENTS

CONTENTS iii

INTRODUCTION 1

ANALYSIS 3

RESULTS 11

CONCLUSIONS 17

ACKNOWLEDGEMENT 19

REFERENCES 20

FIGURE CAPTIONS 21

FIGURES 22

NOMENCLATURE 35

APPENDIX NON-UNITY LEWIS NUMBER 38

INTRODUCTION

This report extends a previous study [1] which investigated the effects of radiation in a combusting boundary layer on a pyrolyzing surface to include the effects of radiation over an inert extension of the pyrolyzing surface in the free flow case only. It also extends previous studies [2,3] to include the effects of radiation on the overall flame length.

The analysis is made for a vertical fuel slab mounted in an adiabatic inert wall. The combusting boundary layer is assumed steady and laminar, with a pyrolysis zone separating the wall and the flame zone. A soot zone is located on the fuel rich side of the flame zone, as shown in Figure 1. Soot and radiating product gases are contained within the boundary layer. A distant black wall maintained at a constant temperature exchanges radiation with the combusting layer through the transparent ambient gas.

The fraction of fuel carbon converted to soot is small [4], allowing the formation and transport of soot to be neglected. The only effect of soot in this model is the increase in radiation heat transfer. The optical thickness of the soot layer has been determined to be small, $\tau < 0.1$, through measurements of the soot volume fraction in boundary layers [1].

The medium is assumed spectrally gray and homogeneous with a constant absorption coefficient. Because most of the radiant energy from the combusting boundary layer is emitted near the flame zone, the value of the absorption coefficient is based on conditions in the soot

layer near the flame zone. Radiation is represented as an equivalent one-dimensional radiant flux which takes into account all radiation towards and from the surface. The optically thin approximation simplifies the radiation terms in the energy equation, and the set of differential equations is solved by numerical methods.

ANALYSIS

The reaction is assumed to be a single step,

$$\nu_f M_f + \nu_o M_o \longrightarrow \nu_p M_p \tag{1}$$

Making the assumptions of a steady flow, a unity Lewis number, transport properties independent of composition and no dissipation, the mass, momentum, enthalpy and species conservation equations describing the model become

$$\frac{\partial(\rho u)}{\partial x} + \frac{\partial(\rho v)}{\partial y} = 0 \tag{2a}$$

$$\rho u \frac{\partial u}{\partial x} + \rho v \frac{\partial u}{\partial y} = \frac{\partial}{\partial y}\left(\mu \frac{\partial u}{\partial y}\right) + g(\rho_\infty - \rho) \tag{2b}$$

$$\rho u \frac{\partial h}{\partial x} + \rho v \frac{\partial h}{\partial y} = \frac{\partial}{\partial y}\left(\frac{k}{c_p}\frac{\partial h}{\partial y}\right) + \dot{q}''' - \frac{\partial q_r}{\partial y} \tag{2c}$$

$$\rho u \frac{\partial Y_i}{\partial x} + \rho v \frac{\partial Y_i}{\partial y} = \frac{\partial}{\partial y}\left(\rho D \frac{\partial Y_i}{\partial y}\right) + \dot{m}''' \tag{2d}$$

where $h = \int_{T_\infty}^{T} c_p dT$. Following Beier's [1] procedure, the combusting boundary layer is assumed optically thin so that the absorption by the medium of its own emitted radiation is neglected. The one-dimensional radiative heat flux and its derivative are given by

$$q_r = \sigma T_w^4 (1 - 2\tau) - \sigma T_{ex}^4 (1 - 2\tau_\delta + 2\tau) + 2\int_0^\tau e_b dt - 2\int_\tau^{\tau_\delta} e_b dt \tag{3a}$$

$$-\frac{\partial q_r}{\partial \tau} = 2\sigma T_w^4 + 2\sigma T_{ex}^4 - 4e_b \tag{3b}$$

where $e_b = \sigma T^4$ = the total emissive power of a blackbody and $T = Ky$, assuming gray diffuse surfaces and a wall emissivity of one.

The boundary conditions over the fuel surface, $0 < x < 1$, are

$$\text{At } y = \delta, \quad u=0,\ h=0,\ Y_o = Y_{o,\infty} \tag{4a}$$

$$\text{At } y = 0. \quad u=0,\ h=h_w,\ \dot{m}_p L = \frac{k}{c_p}\frac{\partial h}{\partial y} - q_r,\ m_p = -\rho D \frac{\partial Y_f / \partial y}{Y_{ff} - Y_{fw}} \tag{4b}$$

Above the fuel, $x > 1$, the mass flux at the wall is zero. Assuming the wall to be adiabatic, the boundary conditions become

$$\text{At } y = \delta, \quad u=0,\ h=0,\ Y_o = Y_{o,\infty} \tag{5a}$$

$$\text{At } y = 0, \quad u=0,\ h=h_w,\ 0 = \frac{k}{c_p}\frac{\partial h}{\partial y} - q_r,\ 0 = \frac{\partial Y_f}{\partial y} \tag{5b}$$

The source terms $\dot{q}'''$ and $\dot{m}'''$ in equations (2c) and (2d) can be eliminated by defining the enthalpy-oxygen Shvab-Zeldovich variable

$$\gamma = -\frac{h}{Q} - \frac{Y_o}{\nu_o M_o} \tag{6a}$$

and the fuel-oxygen Shvab-Zeldovich variable

$$\beta = \frac{Y_f}{\nu_f M_f} - \frac{Y_o}{\nu_o M_o} \tag{6b}$$

The normalized variables have the forms

$$J_\gamma = \frac{\gamma - \gamma_\infty}{\gamma_w - \gamma_\infty} \qquad \text{and} \qquad J_\beta = \frac{\beta - \beta_\infty}{\beta_w - \beta_{w_0}} \tag{7}$$

where β_{w_0} represents the value of β at the wall when radiation is neglected and is determined by

$$Y_{fw_0} = (Y_{ft}B - sY_{o,\infty}) \;/\; (\,1 + B\,) \tag{8}$$

and equation (6b).

Using the definition of the enthalpy and equations (6) and (7), expressions for the enthalpy and temperature profiles are developed

$$(h/h_w) = \begin{cases} D_c - (D_c - 1)J_\gamma & , \; y \leqslant y_{fl} \qquad (9a) \\ \\ -\,(D_c - 1)J_\gamma + D_c(1 + r^{-1})J_\beta & , \; y \geqslant y_{fl} \qquad (9b) \end{cases}$$

$$\theta = T/T_\infty = 1 + (\theta_w - 1)(h/h_w) \tag{10}$$

Equations (2), (4) and (5) are transformed from (x.y) coordinates to the nondimensional coordinates (ξ,η) by defining

$$\xi = (x/\ell)^{1/4} \qquad \text{and} \qquad \eta = \frac{Gr_x^{1/4}}{2^{1/2}x}\int_0^y (\rho/\rho_\infty)\,dy \tag{11}$$

Defining the stream function such that

$$\frac{\partial \psi}{\partial y} = \frac{\rho u}{\rho_\infty} \qquad \text{and} \qquad \frac{\partial \psi}{\partial x} = -\frac{\rho v}{\rho_\infty} \tag{12}$$

satisfies equation (2a). The transformed stream function is assumed to be of the form

$$\psi = 2^{3/2} \nu_\infty Gr^{1/4} f(\eta) \tag{13}$$

Assuming ρT is a constant, the problem is fully described by the transformed momentum, enthalpy and species conservation equations and the transformed boundary conditions

$$f''' + 3ff'' - 2(f')^2 + (h/h_w) = \xi\left(f'\frac{\partial f'}{\partial \xi} - f''\frac{\partial f}{\partial \xi}\right) \tag{14a}$$

$$J_\gamma'' + 3PrfJ_\gamma' = Pr\,\xi\left(f'\frac{\partial J_\gamma}{\partial \xi} - J_\gamma'\frac{\partial f}{\partial \xi}\right) - \frac{N_1 N_2^2 \xi^2 \theta \;\; \partial Q_r}{(\theta_w - 1)(D_c - 1)\;\partial T} \tag{14b}$$

$$J_\beta'' + 3PrfJ_\beta' = Pr\,\xi\left(f'\frac{\partial J_\beta}{\partial \xi} - J_\beta'\frac{\partial f}{\partial \xi}\right) \tag{14c}$$

<u>$0 \leq \xi \leq 1$</u>

$$\begin{aligned} &\text{At } \eta \to \infty, \quad f' = 0,\ J_\gamma = 0,\ J_\beta = 0 \\ &\text{At } \eta = 0, \quad f' = 0,\ J_\gamma(\xi = 0) = 1,\ J_\beta(\xi = 0) = 1,\ J_\beta' = 0, \\ &\qquad J_\gamma' = \frac{Pr}{B}\left(3f + \xi\frac{\partial f}{\partial \xi}\right) - \frac{N_2 \xi Q_r}{(\theta_w - 1)(D_c - 1)} \end{aligned} \tag{15}$$

<u>$\xi \geq 1$</u>

$$\begin{aligned} &\text{At } \eta \to \infty, \quad f' = 0,\ J_\gamma = 0,\ J_\beta = 0 \\ &\text{At } \eta = 0, \quad f' = 0,\ J_\beta' = 0,\ J_\gamma' = -\frac{N_2 \xi Q_r}{(\theta_w - 1)(D_c - 1)},\ 3f + \xi\frac{\partial f}{\partial \xi} = 0 \end{aligned} \tag{16}$$

where $Q_r = q_r / \sigma T_\infty^4$, and the radiation parameters are defined as

$$N_1 = \frac{k_\infty K}{\sigma T_\infty^3} \qquad \text{and} \qquad N_2 = \frac{2^{1/2} \sigma T_\infty^3}{k_\infty} \frac{\ell}{Gr_\ell^{1/4}} \tag{17}$$

Using equation (12), the local and total pyrolysis rates at the wall are

$$-\frac{2^{1/2} x}{\nu_\infty \rho_\infty Gr_x^{1/4}} \dot{m}_p(x) = 3f(\xi,0) + \xi \frac{\partial f}{\partial \xi}(\xi,0) \tag{18a}$$

$$-\frac{1}{2^{3/2} \nu_\infty \rho_\infty Gr_x^{1/4}} \dot{M}_p(x) = f(\xi,0) \qquad , \; 0 \leq x \leq \ell \tag{18b}$$

where $\dot{M}_p = \int_0^x \dot{m}_p dx$.

The excess pyrolyzate is the downstream flux of fuel between the wall and flame

$$\dot{m}_e(x) = \int_0^{y_{fl}} (\rho u Y_f)_x dy \tag{19}$$

Transforming $\dot{m}_e(x)$ to (ξ,η) coordinates and normalizing on $\dot{m}_p(x)$ in equation (18b) yields the unburned fraction of the total fuel pyrolyzate

$$\frac{\dot{m}_e(\xi)}{\dot{m}_p(\xi)} = \frac{BY_{fl}}{B+r+1} \left[\frac{r f(\xi,\eta_{fl})}{f(\xi,0)} - r - \frac{(r+1)}{f(\xi,0)} \int_0^{\eta_{fl}} f' J_\gamma d\eta \right] \tag{20}$$

Using equation (9), the heat flux at the wall due to conduction is

$$q_c(\xi,0) = \frac{Gr_x^{1/4}}{2^{1/2}x} \frac{\nu_\infty \rho_\infty}{Pr} J_\gamma'(\xi,0) \tag{21}$$

Using equations (6b) and (7) and the definition of the mass consumption number, r

$$r = \frac{Y_{o,\infty}}{Y_{fw_o}} \frac{\nu_f M_f}{\nu_o M_o} \tag{22}$$

the solution for J_β at the flame is

$$J_{\beta fl} = r/(1+r) \tag{23}$$

The flame height is found by setting J_β at the wall equal to J_β at the flame

$$J_\beta(\xi,0) = J_{\beta fl} = r/(1+r) \qquad \text{at } \xi = \xi_{fl} \tag{24}$$

Solutions were computed for a Prandtl number of 0.73 using finite difference methods. Two-point backward differences replaced the derivative, ie, $\partial f/\partial \xi = (f_m - f_{m-1})/\Delta\xi$, to give a set of coupled ordinary equations at each streamwise station. Newman's [5]

iterative, finite difference method was used to solve this system of non-linear, ordinary differential equations. The streamwise step size, $d\xi$, was set at 0.05 along the pyrolyzing surface. At $\xi=1.0$, the step size was decreased to $d\xi=0.0005$ for ten steps to maintain accuracy in the extended flame region. The step size was set at $d\xi=0.005$ along the remainder of the inert wall. The computational time varied from approximately 20 to 60 minutes per run.

A combusting boundary layer without radiation at $\xi=0$ is described by equations (14),(15) and (16). Thus the deviation of surface values and gradients with ξ is the result of radiative effects.

Assuming a Prandtl number of 0.73 and a unity Lewis number, a total of seven parameters describe a radiative combusting boundary layer. These parameters are: r, the mass consumption number; B, the mass transfer number; D_c, the dimensionless heat of combustion; N_1, the soot parameter; N_2, the length parameter; θ_w, the dimensionless pyrolysis temperature and θ_{ex}, the dimensionless distant wall temperature. To study the effects of the parameters individually, a typical synthetic polymer burning in air was modeled and r, B, D_c, N_1, N_2, θ_w and θ_{ex} were each varied over a typical range while holding the remaining six parameters constant. The "standard case" parameter values and ranges that were examined are

$r = 0.1$	$0.1 < r < 0.25$
$B = 1.0$	$1.0 < B < 10.0$
$D_c = 5.0$	$5.0 < D_c < 10.0$

$N_1 = 0.02$	$0.02 < N_1 < 0.30$
$N_2 = 0.05$	$0.025 < N_2 < 0.10$
$\theta_w = 2.0$	$1.25 < \theta_w < 3.0$
$\theta_{ex} = 1.0$	$1.0 < \theta_{ex} < 4.0$

The parameters were varied to measure their effects on the unburned fraction of pyrolyzate, the mass pyrolysis rate and the net radiative flux. These effects explained the differences in the predicted radiative flame lengths. The results were used to determine an approximate expression for the radiative flame height as a function of the seven dimensionless parameters describing a combusting boundary layer.

RESULTS

The surface temperature characteristics of a typical fuel/inert system are shown in Figure 2. The temperature remains constant at 600 K over the pyrolyzing surface, $0 < \xi < 1$, and then rises sharply at the inert wall, peaking at about 760 K . The sudden increase in temperature is due to the elimination of blowing at the surface when $\xi > 1$. The incoming energy to the wall heats the surface and, because the wall is assumed to be adiabatic, the energy radiated out from the wall must equal the energy conducted to the wall .

Previous studies [2,3] have shown the dominant parameter influencing the unburned fraction of pyrolyzate to be r, the mass consumption number. This remains true for the radiative model, as shown in Figure 3. Increasing r corresponds to increasing the available oxygen relative to the required oxygen, and the flame moves towards the pyrolyzing surface to compensate. The downstream flux of fuel between the wall and the flame, $\dot{M}_e$, decreases, causing the unburned fraction of pyrolyzate, $\dot{M}_e/\dot{M}_p$ to decrease.

Beyond the end of the pyrolyzing surface, $\xi > 1$, $\dot{M}_e/\dot{M}_p$ decreases rapidly because the inert wall does not contribute pyrolyzate and the unburned pyrolyzate is being consumed. The flame height is measured as the point along the inert wall where $\dot{M}_e/\dot{M}_p$ goes to zero.

The mass consumption number, B, strongly affects the mass pyrolysis rate, $-f(\xi,0)$, as found in the nonradiative solution. An increase in B corresponds to more mass transfer and results in a higher pyrolysis rate as shown in Figure 4.

The normalized net radiation from the wall, Q_r, is directly affected by four parameters: D_c, the dimensionless heat of combustion, N_1, the soot parameter, θ_w, the pyrolysis temperature, and θ_{ex}, the distant wall temperature.

The effects of D_c and N_1 on Q_r are shown in Figure 5. Increasing D_c raises the flame temperature, and the net radiation from the wall, Q_r, decreases. Along the adiabatic inert wall the conduction to the wall must equal the radiation from the wall. The high flame temperature increases the conduction to the wall, causing a large radiative flux from the wall for $\xi > 1$. The amount of soot in the flame increases when N_1 is increased, causing the net radiation from the pyrolyzing surface to decrease. Due to the energy loss from the radiating soot, the flame temperature decreases and thus the conduction to the wall decreases. The loss of energy due to decreased conduction is greater than the increased radiation from the flame, resulting in a net decrease in the radiation from the adiabatic wall. Because D_c and N_1 control the radiation from the flame, they do not affect Q_r at $\xi = 0$, where the thickness of the radiating soot layer goes to zero.

The net radiation is strongly dependent on the pyrolysis and distant wall temperatures, as shown in Figure 6. A higher pyrolysis temperature increases the radiation from the wall, while a higher distant wall temperature, representing a nearby fire, causes a large decrease in Q_r due to the energy radiated from the distant fire to the pyrolyzing surface.

An approximate equation for the flame length of a wall-mounted

free-flow flame, neglecting radiation, has been developed by Pagni [3]

$$X_{fl}^{*} = 0.24\ [(1+r^{-1})r^{-0.16}(1+B^{-1})B^{-0.06}\ln(1+B)D_c^{-0.03}]^{4/3} \qquad (25)$$

Flame lengths predicted with equation (25) and by the results of the radiative model for three liquid fuels, n-heptane, cyclohexane, and iso-octane, and three solid fuels, cellulose, polymethylmethacrylate (PMMA), and polystyrene, are listed in Table 1 . The length of the pyrolyzing surface was taken as ℓ=0.01 m and the distant wall temperature was set at θ_{ex}=1.0 in all cases.

Including radiation in the model results in an increase in the predicted flame lengths for the liquid fuels and a decrease in the predicted flame lengths for the solid fuels. The liquid fuels have low pyrolysis temperatures of approximately 375 K and high D_c values, indicating high flame temperatures. For a liquid fuel, the energy lost from the pyrolyzing surface to the ambiance at 300 K is less than the energy gained from the flame and the net radiative flux is toward the pyrolyzing surface. The increased energy to the wall increases the mass pyrolysis rate. The flame moves away from the surface to compensate, and the unburned pyrolyzate increases. The result is a longer flame. The solid fuels have higher pyrolysis temperatures, ranging from about 650 K to 850 K, and lower values of D_c. The net radiative flux is away from the pyrolyzing surface, causing the flame to move toward the wall, and the predicted flame length for a solid fuel burning in air decreases when radiation is included in the model.

Because the net radiative flux is towards the pyrolyzing surface for a liquid fuel, increasing the length of the pyrolyzing surface allows more radiative energy to reach the fuel and increases the flame length. The opposite is true for a solid fuel at ambient conditions. Increasing the fuel length decreases the nondimensional flame length. Table 2 lists the predicted flame lengths for a typical liquid fuel, n-heptane, and a typical solid fuel, cellulose, for fuel lengths of 1 cm. and 5 cm.

Figure 7 shows the variation of the radiative flame length with r and B . Because increasing r results in a decrease in the unburned fraction of pyrolyzate, less fuel is available above the pyrolyzing surface and the flame length decreases. Increasing B increases the mass pyrolysis rate, thus increasing the flame length.

In Figure 8 the flame length is plotted for varying D_c and N_1 values. As discussed earlier, increasing either D_c or N_1 decreases the net radiation from the pyrolyzing surface. The pyrolysis rate increases, moving the flame away from the wall and the flame length increases.

The variation of the flame length when the pyrolysis temperature, θ_w, is varied is shown in Figure 9 . In Figure 6 it was shown that increasing θ_w increases the net radiation from the wall. This results in a lower pyrolysis rate and a lower flame length.

It was also shown in Figure 6 that increasing the distant wall temperature, θ_{ex}, to represent a nearby fire dramatically increases the amount of radiation towards the pyrolyzing surface. The flame length is expected to also increase dramatically, and this is verified

by the results shown in Figure 10 .

An empirical expression for the radiative flame length has been determined using the results of the radiative model

$$X^*_{fl} = 10^{-2} \exp[-34.7r^3+43.0r^2-20.6r+4.16][\ln(B+0.5)+2.33]$$
$$(N_1^2-0.93N_1-0.28)(0.36-N_2)(\theta_w^2-2.14\theta_w-11.3)$$
$$(\theta_{ex}^3-3.64\theta_{ex}^2+4.82\theta_{ex}+0.77)(D_c+6.52) \qquad (26)$$

This expression incorporates the seven dimensionless parameters describing a combusting boundary layer, and applies to solid fuels for the free flow case with the following restrictions

$$0.1 < r < 0.6$$
$$1.0 < B < 10.0$$
$$5.0 < D_c < 10.0$$
$$0.02 < N_1 < 0.30$$
$$0.025 < N_2 < 0.10$$
$$10^{-5} < N_1 N_2^2 < 10^{-4}$$
$$2.0 < \theta_w < 3.0$$
$$1.0 < \theta_{ex} < 4.0$$

Equation (26) has been used to predict the radiative flame lengths of PMMA in free flow for varying ambient oxygen mass fractions. Figure 11 shows the predicted radiative and nonradiative flame heights for fuel lengths of 1 and 2 cm.s. Values of the pyrolysis temperature were calculated using the kinetic data given in

Sohrab and Williams [6], and θ_w has also been plotted against $Y_{o,\infty}$ in Figure 11 . The results indicate that there is an oxygen concentration, depending on N_2, above which the addition of radiation to the model increases the predicted flame lengths for solid fuels. These results are verified by Figure 3 of Kinoshita and Pagni [2], where in the forced flow case for fuel lengths of 1.3 and 1.6 cm.s, the experimentally determined flame lengths, corresponding to the radiative flame lengths, become greater than the nonradiative flame lengths at approximately 30% ambient oxygen mass fraction. Our cross-overs occur at higher oxygen mass fractions because our calculations are for free flow.

CONCLUSIONS

Assuming a wall emissivity of unity and a Prandtl number of 0.73, seven dimensionless parameters remain to describe an optically thin combusting boundary layer with radiation. As in the non-radiative case, a mass consumption number, r, and a mass transfer number, B, control the fraction of unburned gases escaping downstream and the mass pyrolysis rate, respectively. D_c, a dimensionless heat of combustion, controls the flame temperature and thus has a significant effect on the net radiative flux.

The radiative model introduces four parameters which directly affect the net radiation at the wall: N_1, a soot or absorption coefficient, N_2, a length parameter, θ_w, a dimensionless pyrolysis temperature, and θ_{ex}, a dimensionless distant wall temperature which characterizes any external radiative flux.

Because the liquid fuels studied have net radiative fluxes towards the fuel, including radiation in the model increases the predicted flame lengths. Increasing the length parameter, N_2, also causes an increase in the flame lengths for the liquid fuels. The solid fuels have net radiative fluxes away from the fuel due to their higher surface temperatures and lower flame temperatures. Including radiation in the model decreases the predicted flame lengths for solid fuels. The flame to surface conductive heat flux decreases downstream as the boundary layer grows, causing the net radiative flux from the solid fuels to increase downstream, under our assumption of an adiabatic inert wall. Increasing the length of a solid pyrolyzing

surface thus increases the radiative heat flux from the surface, decreases the mass pyrolysis rate, and consequently decreases the flame length.

An approximate expression incorporating the seven dimensionless parameters has been determined for the radiative flame length of solids in free flow. The expression has been determined to be accurate to within 5% for the ranges of the parameters given.

The next step in this work is to test the radiative model predictions experimentally. An apparatus consisting of three thin film temperature gauges mounted in an inert wall has been constructed so that the flame length and the net radiative flux at various downstream locations can be determined. Both solid and liquid fuels will be tested with lengths varying from 1 to 5 cm.s.

Additional theoretical work will first consist of determining an approximate empirical expression for the radiative flame height of a liquid fuel in free flow. An extension of the work to forced and mixed flows should follow. A preliminary study of the non-unity Lewis number is reported in the Appendix. Eliminating the assumption of laminar flow to include the effects of turbulence is also desirable.

It is hoped that the empirical expression for the radiative flame length of a solid fuel given in this report will guide manufacturers in material selection and encourage the development of a simple test for measuring flame heights as a relative index of material fire hazard.

ACKNOWLEDGEMENT

This work was supported by the Center for Fire Research in the U.S.D.O.C. National Bureau of Standards under Grant No. NB 80 NAG-E6839 which was administered by the U.S. Department of Energy under Contract No. W-7405-ENG-48 at the Lawrence Berkeley Laboratory of the University of California.

REFERENCES

1. Beier, R. A , "Soot and Radiation in Combusting Boundary Layers", Ph.D. Dissertation, Mechanical Engineering Dept., University of California, Berkeley, 1981

2. Kinoshita, C. M., and Pagni, P. J., "Laminar Wake Flame Heights", ASME Journal of Heat Transfer. Vol. 102. pp. 104-109, 1980

3. Pagni, P. J., "Diffusion Flame Analyses", Fire Safety Journal, 3, pp. 273-285 1980/81

4. Bard, S., "Diffusion Flame Particulate Volume Fractions", Ph.D. Dissertation, Mechanical Engineering Dept., University of California, Berkeley, 1980

5. Newman, J., "Numerical Solution of Coupled, Ordinary Differential Equations", Industrial and Engineering Chemistry Fundamentals, Vol. 7, pp. 514-517, 1968

6. Sohrab, S. H., and Williams, F. A., "Extinction of Diffusion Flames Adjacent to Flat Surface of Burning Polymers", Applied Mechanics and Engineering Sciences Dept., University of California, San Diego, 1981

7. Kassoy, D. R., and Williams, F. A., "Variable Property Effects on Liquid Droplet Combustion", AIAA Journal, Vol. 6, No. 10, October 1968

FIGURE CAPTIONS

1 System schematic of steady, two-dimensional, wall-mounted, free flow diffusion flame on a vertical pyrolyzing fuel slab.

2 The normalized wall temperature vs. the streamwise distance for $r = 0.1$, $B = 1$, $D_c = 5$, $N_1 = 0.02$, $N_2 = 0.05$, $\theta_w = 2.0$, $\theta_{ex} = 1.0$

3 The unburned fraction of pyrolyzate vs. the streamwise distance for varying values of r, where $B = 1$, $D_c = 5$, $N_1 = 0.02$, $N_2 = 0.05$, $\theta_w = 2.0$, $\theta_{ex} = 1.0$

4 The mass pyrolysis rate at the fuel vs. the streamwise distance for varying values of B, where $r = 0.1$, $D_c = 5$, $N_1 = 0.02$, $N_2 = 0.05$, $\theta_w = 2.0$, $\theta_{ex} = 1.0$

5 The normalized net radiative flux from the wall vs. the streamwise distance for varying values of D_c and N_1, where $r = 0.1$, $B = 1$, $N_2 = 0.05$, $\theta_w = 2.0$, $\theta_{ex} = 1.0$

6 The normalized net radiative flux from the wall vs. the streamwise distance for varying values of θ_w and θ_{ex}, where $r = 0.1$, $B = 1$, $D_c = 5$, $N_1 = 0.02$, $N_2 = 0.05$

7 The variation of the normalized radiative flame length with r and B, where $D_c = 5$, $N_1 = 0.02$, $N_2 = 0.05$, $\theta_w = 2.0$, $\theta_{ex} = 1.0$

8 The variation of the normalized radiative flame length with D_c and N_1, where $r = 0.1$, $B = 1$, $N_2 = 0.05$, $\theta_w = 2.0$, $\theta_{ex} = 1.0$

9 The variation of the normalized radiative flame length with θ_w, where $r = 0.1$, $B = 1$, $D_c = 5$, $N_1 = 0.02$, $N_2 = 0.05$, $\theta_{ex} = 1.0$

10 The variation of the normalized radiative flame length with θ_{ex}, where $r = 0.1$, $B = 1$, $D_c = 5$, $N_1 = 0.02$, $N_2 = 0.05$, $\theta_w = 2.0$

11 The variation of the predicted radiative and nonradiative flame lengths and θ_w with ambient oxygen mass fraction for 1 and 2 cm. slabs of PMMA in free flow, where $r = 0.22$, $B = 1.5$, $D_c = 5.1$, $N_1 = 0.021$, $N_2 = 0.049$, $\theta_{ex} = 1.0$

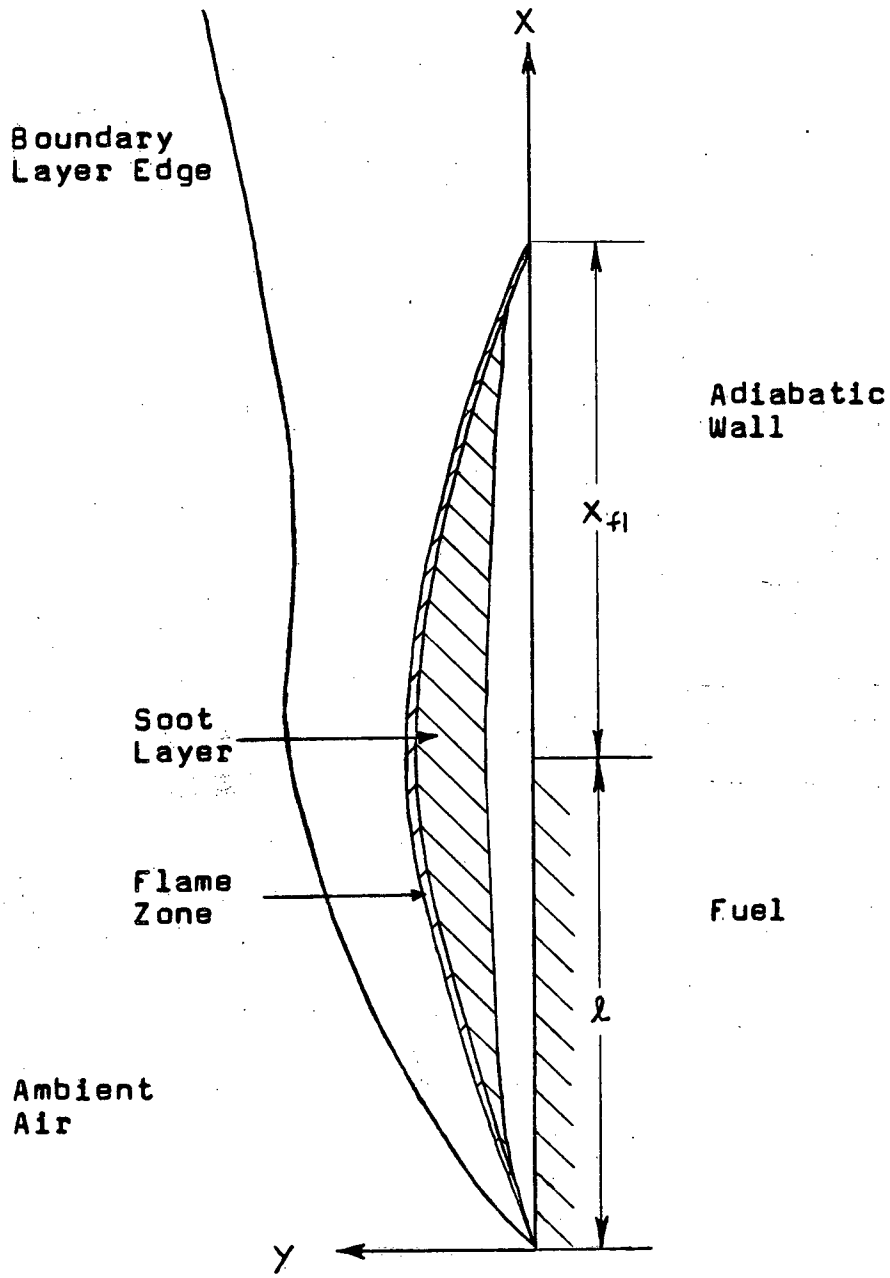
X
Boundary
Layer Edge
Adiabatic
Wall
X_{fl}
Soot
Layer
Flame
Zone
Fuel
ℓ
Ambient
Air
Y

Figure 1

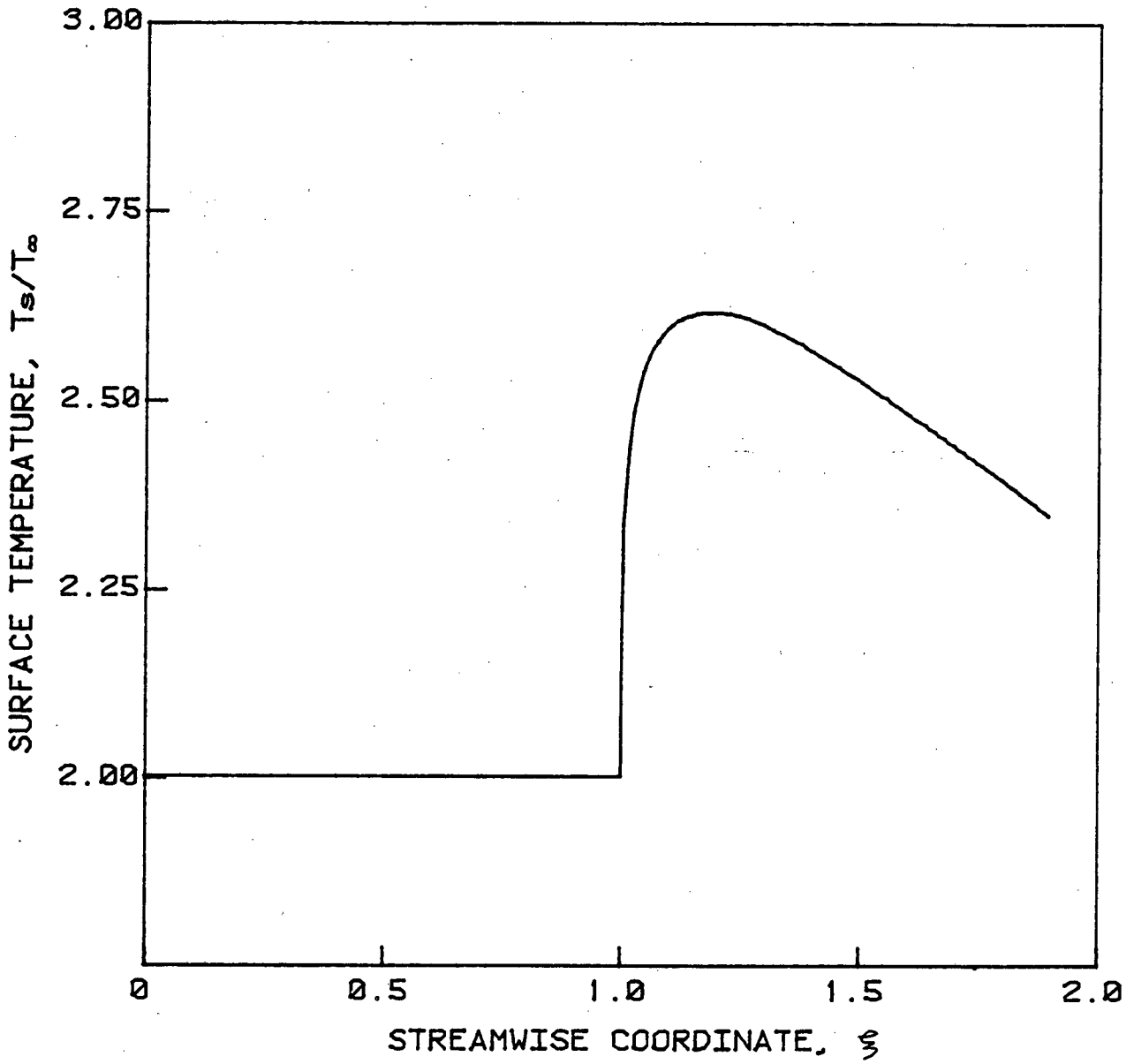
3.00
2.75
2.50
2.25
2.00
SURFACE TEMPERATURE, T_s/T_∞
0
0.5
1.0
1.5
2.0
STREAMWISE COORDINATE, ξ

Figure 2

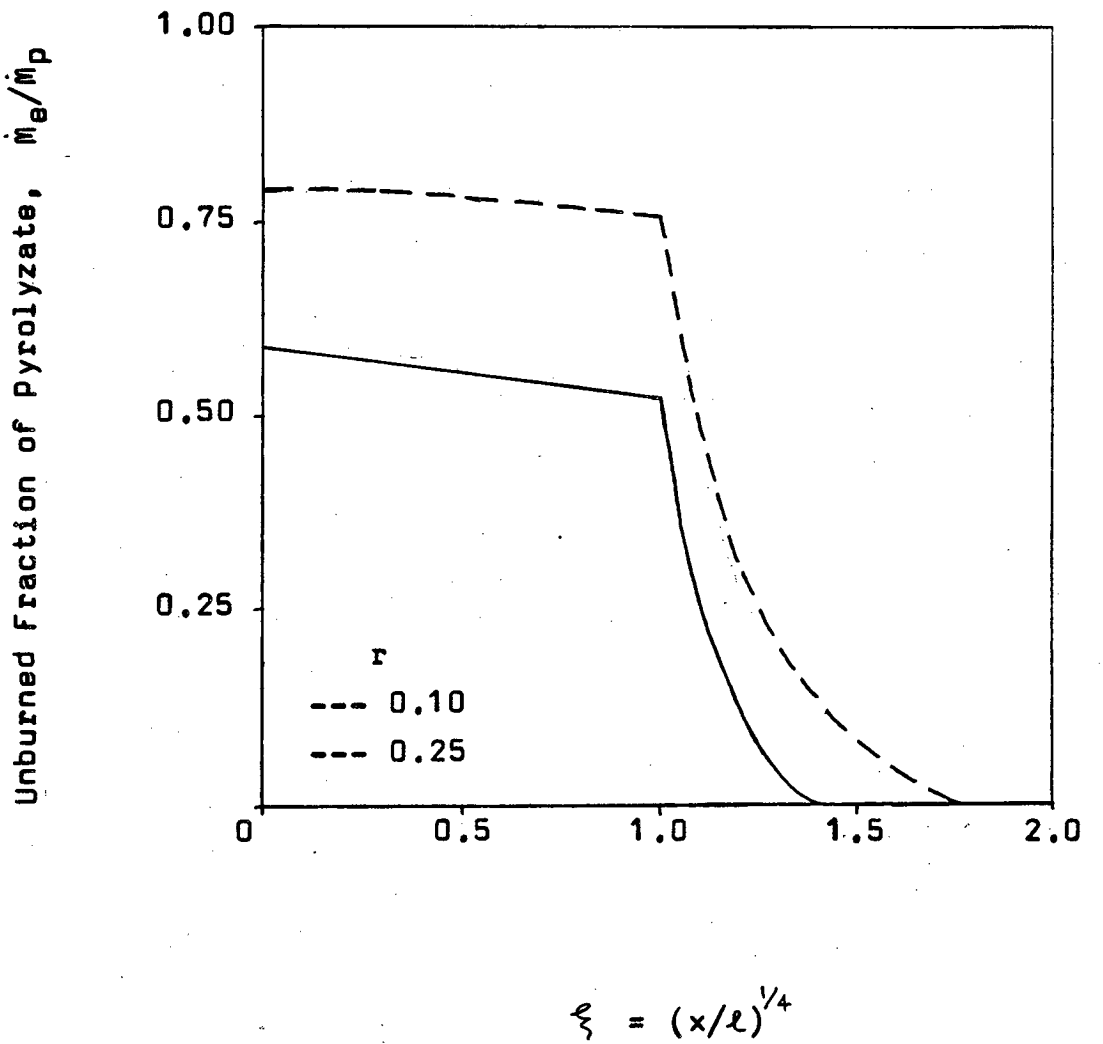
1.00
0.75
0.50
0.25
0
0.5
1.0
1.5
2.0
Unburned Fraction of Pyrolyzate, $\dot{m}_B/\dot{m}_p$
r
--- 0.10
--- 0.25
$\xi = (x/\ell)^{1/4}$

Figure 3

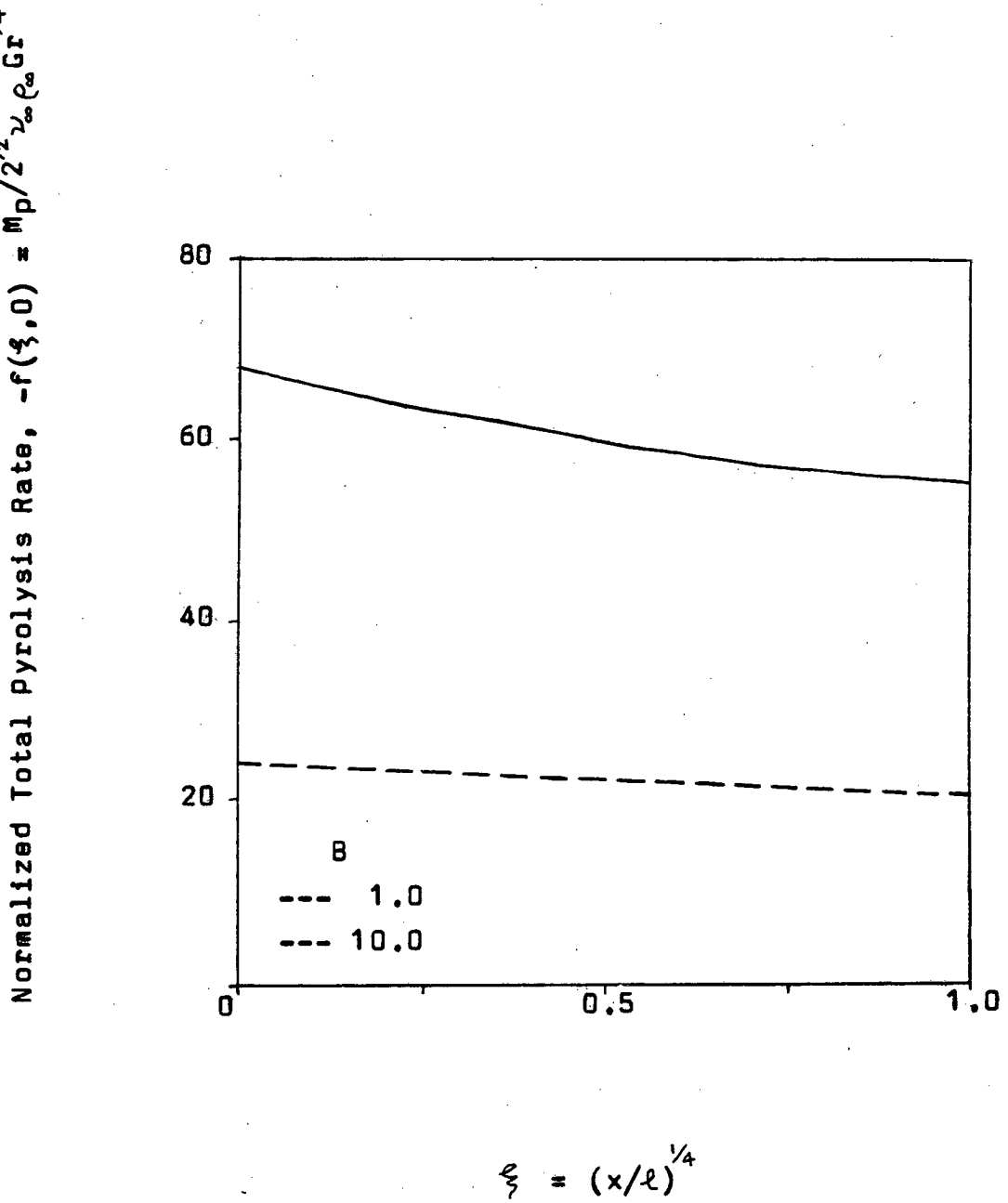
Normalized Total Pyrolysis Rate, $-f(\xi,0) = \dot{M}_p/2^{3/2}\nu_\infty\rho_\infty Gr^{1/4}$
80
60
40
20
0
0.5
1.0
B
--- 1.0
--- 10.0
$\xi = (x/\ell)^{1/4}$

Figure 4

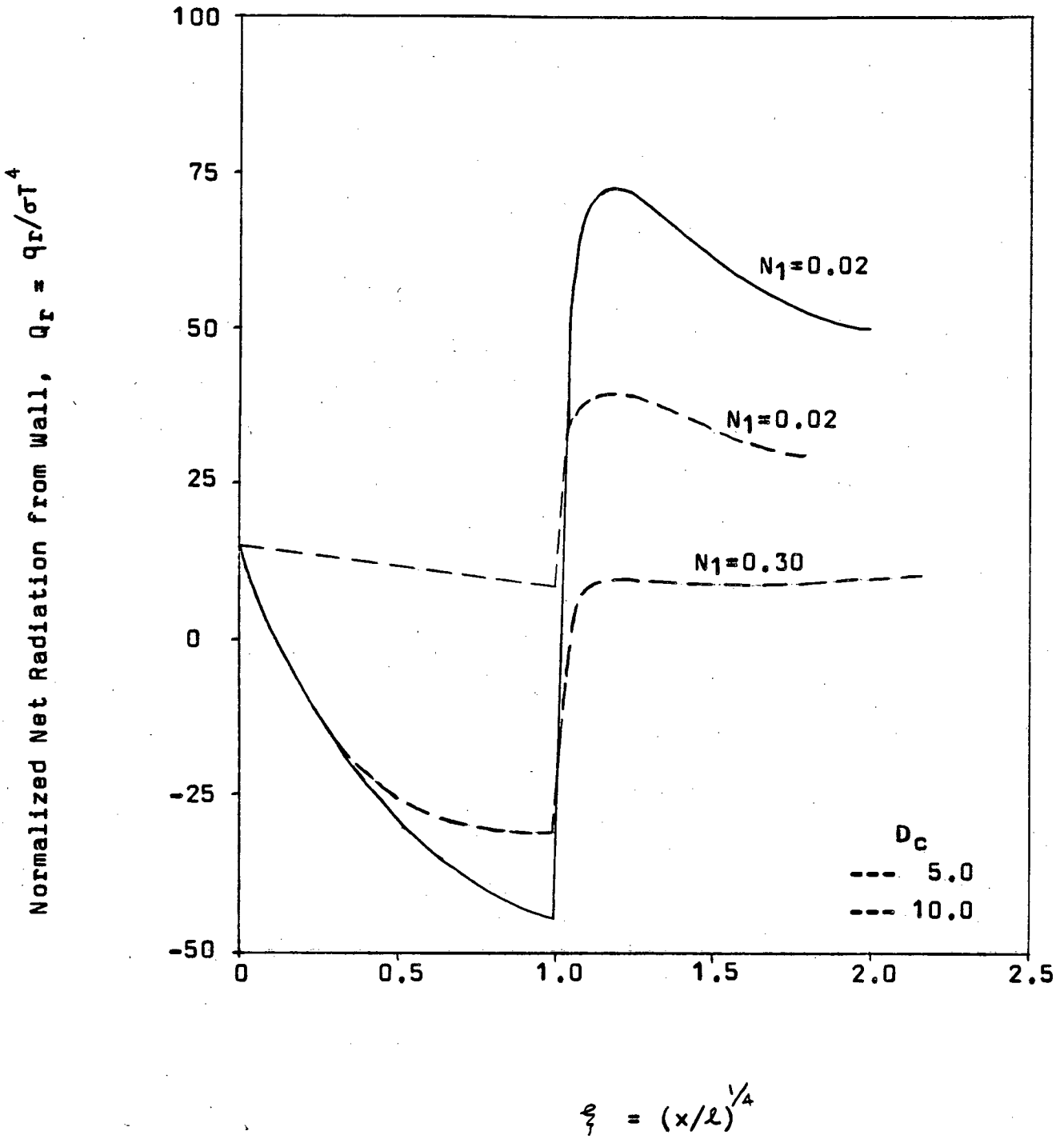
100
75
50
25
0
-25
-50
0
0.5
1.0
1.5
2.0
2.5
Normalized Net Radiation from Wall, $Q_r = q_r/\sigma T^4$
N_1=0.02
N_1=0.02
N_1=0.30
D_c
5.0
10.0
$\xi = (x/\ell)^{1/4}$

Figure 5

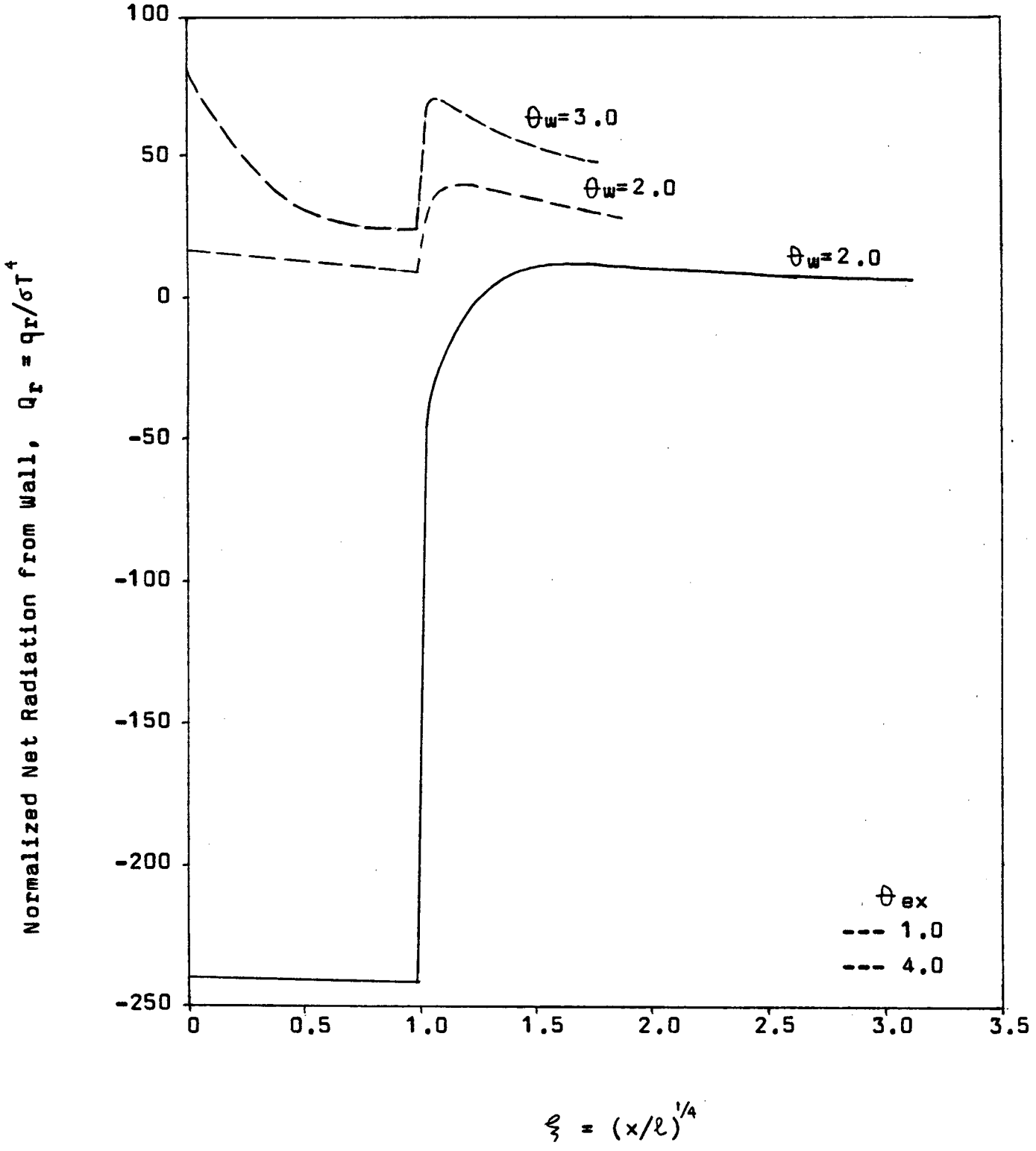
100
50
0
-50
-100
-150
-200
-250
0
0.5
1.0
1.5
2.0
2.5
3.0
3.5
Normalized Net Radiation from Wall, $Q_r = q_r/\sigma T^4$
$\theta_w = 3.0$
$\theta_w = 2.0$
$\theta_w = 2.0$
θ_{ex}
--- 1.0
--- 4.0
$\xi = (x/\ell)^{1/4}$

Figure 6

Material	s	Q_p (kJ/g$_{O_2}$)	L (kJ/g)	T_w (K)	Y_{fw}	f_v ($\times 10^6$)	r	B	D_c	N_1 ($\times 10^2$)	N_2 ($\times 10^2$)	X^*_{fl} non-rad.	X^*_{fl} rad.
Liquids													
n-heptane	0.28	13	0.51	370	0.8	0.3	0.08	5.6	29	1.6	7.4	30	37
cyclohexane	0.29	13	0.47	350	0.8	0.5	0.08	6.1	37	2.6	8.1	30	44
iso-octane	0.29	13	0.45	370	0.8	0.6	0.08	6.3	28	3.2	7.4	32	48
Solids													
cellulose	0.84	14	3.5	650	0.3	0.5	0.60	0.8	6.9	2.7	0.34	1.4	1.2
PMMA	0.52	13	1.6	700	0.5	0.4	0.22	1.5	5.1	2.1	4.9	5.2	4.1
polystyrene	0.33	13	1.7	850	0.5	6	0.14	1.3	4.1	31	5.1	9.3	9.0

Table 1. Predicted nonradiative and radiative flame lengths and ideal material properties for liquid and solid fuels, where T_∞ = 298 K, $Y_{O,\infty}$ = 0.23, c_p = 1.3 kJ/kgK, k_∞ = 0.026 W/mK, ν_∞ = 1.5x10^{-5} m^2/s, ρ_∞ = 1.2 kg/m^3, $T_{ex} = T_\infty$ and ℓ = 0.01 m.

Fuel	ℓ (m)	N_2 ($\times 10^2$)	X_{fl}^*
n-heptane	0.01	7.4	37
	0.05	11	45
cellulose	0.01	5.2	0.89
	0.05	7.8	0.71

Table 2. Predicted radiative flame lengths for n-heptane and cellulose with ℓ = 1 and 5 cm.s

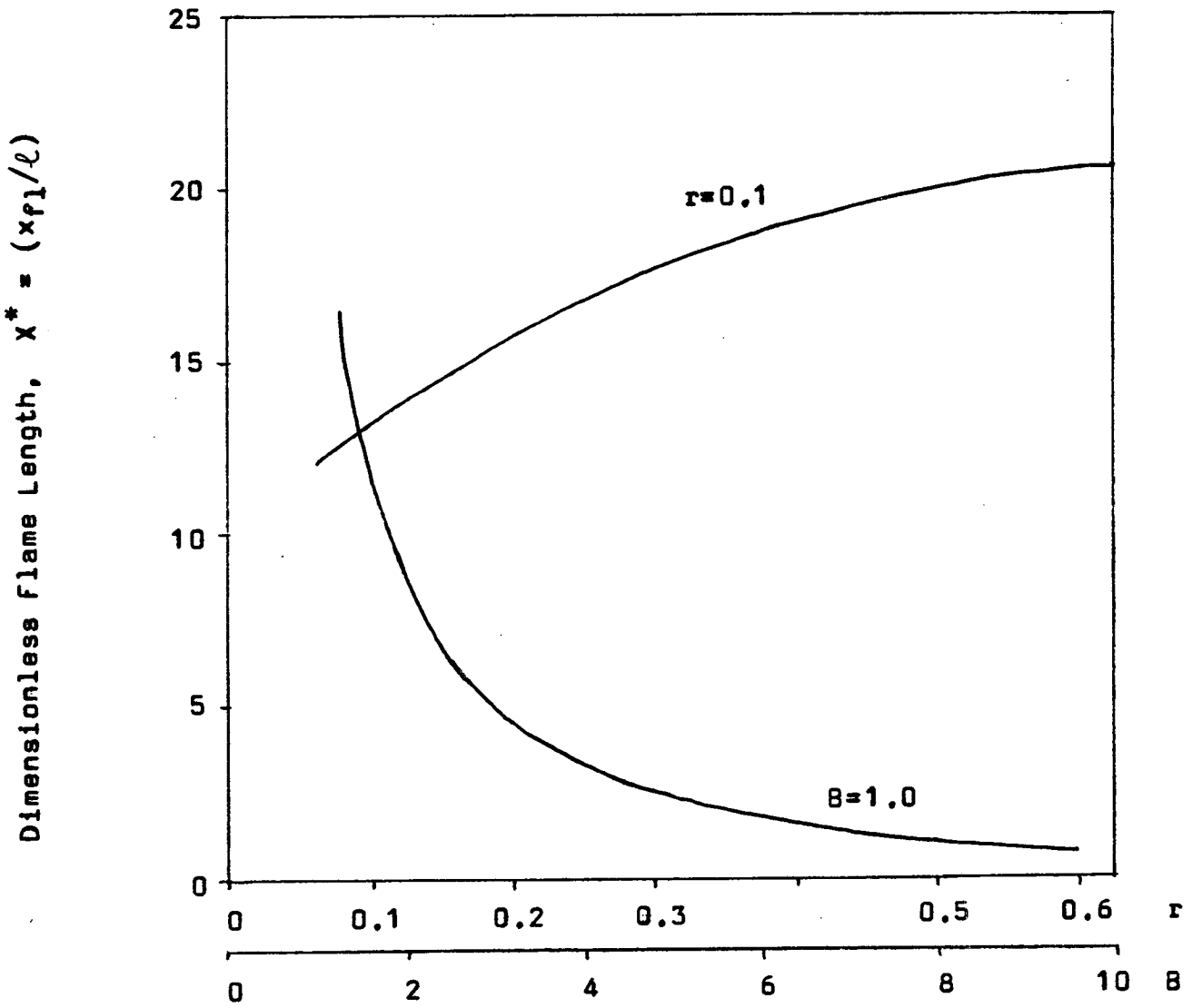
Dimensionless Flame Length, $X^* = (x_{fl}/\ell)$
25
20
15
10
5
0
r=0.1
B=1.0
0
0.1
0.2
0.3
0.5
0.6
r
0
2
4
6
8
10
B

Figure 7

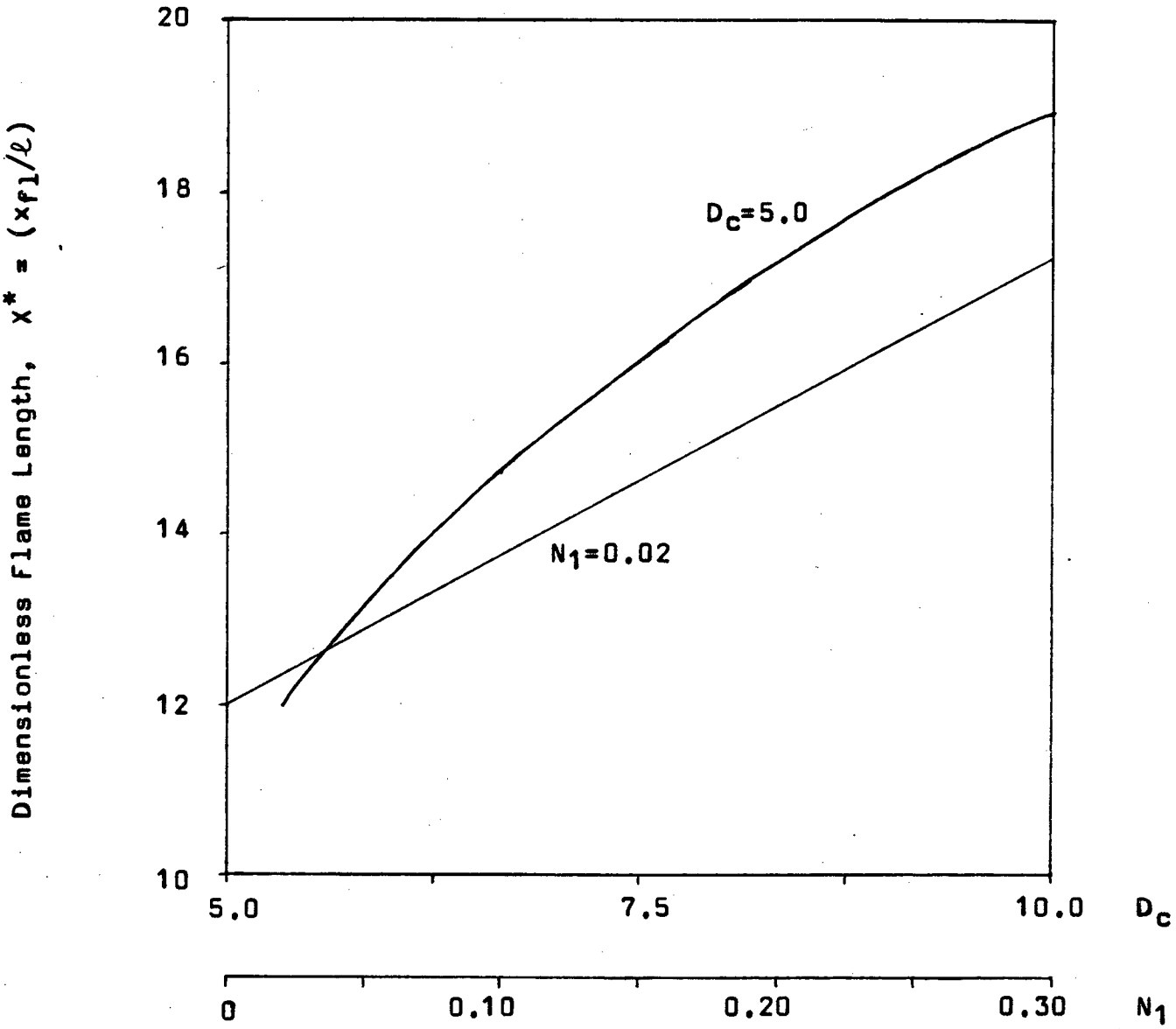
20
18
16
14
12
10
Dimensionless Flame Length, $X^* = (x_{f1}/\ell)$
D_c=5.0
N_1=0.02
5.0
7.5
10.0
D_c
0
0.10
0.20
0.30
N_1

Figure 8

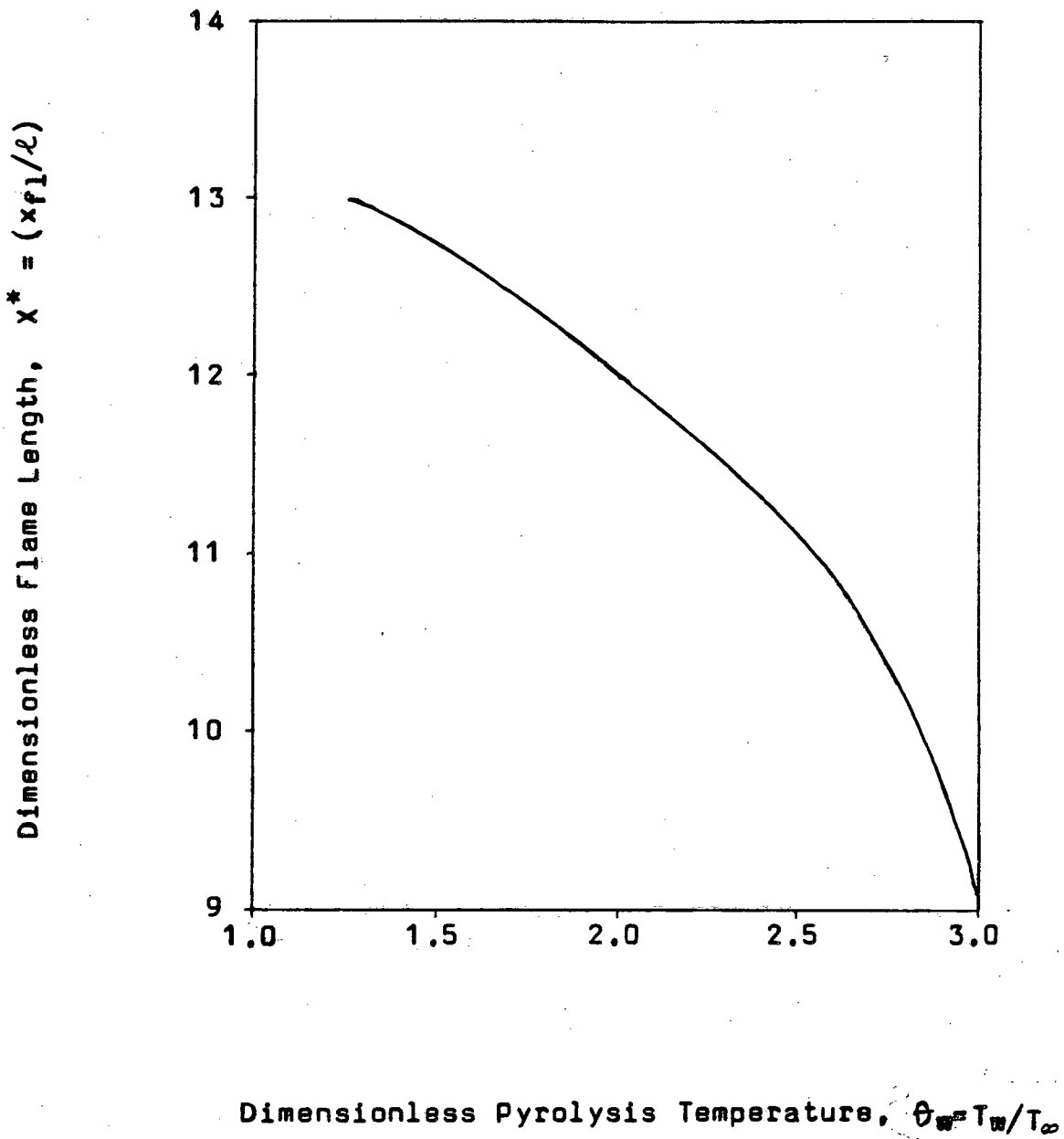
14
13
12
11
10
9
1.0
1.5
2.0
2.5
3.0
Dimensionless Flame Length, $X^* = (x_{fl}/\ell)$
Dimensionless Pyrolysis Temperature, $\theta_w = T_w/T_\infty$

Figure 9

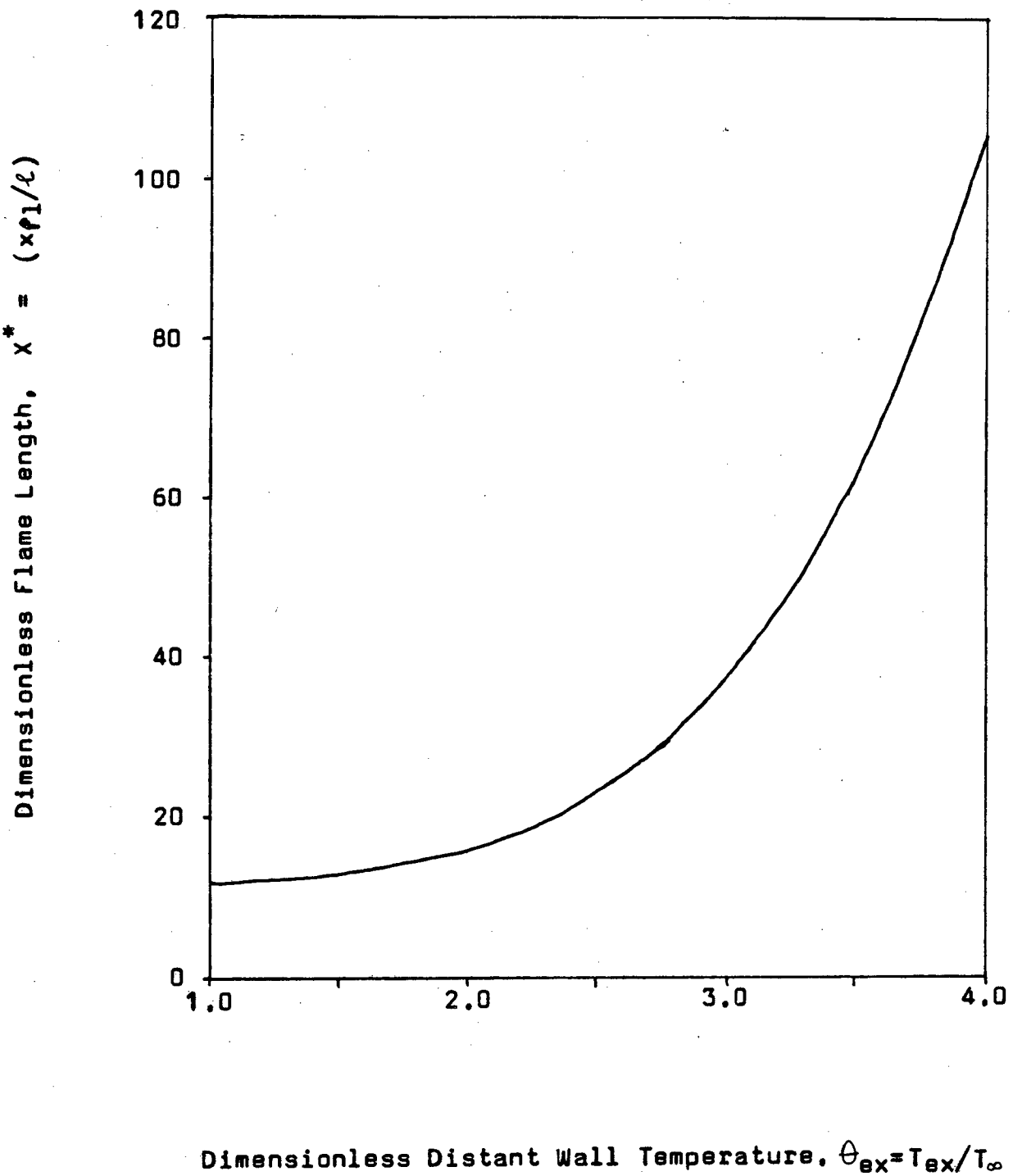
120
100
80
60
40
20
0
1.0
2.0
3.0
4.0
Dimensionless Flame Length, $x^* = (x\rho_1/\ell)$
Dimensionless Distant Wall Temperature, $\theta_{ex}=T_{ex}/T_\infty$

Figure 10

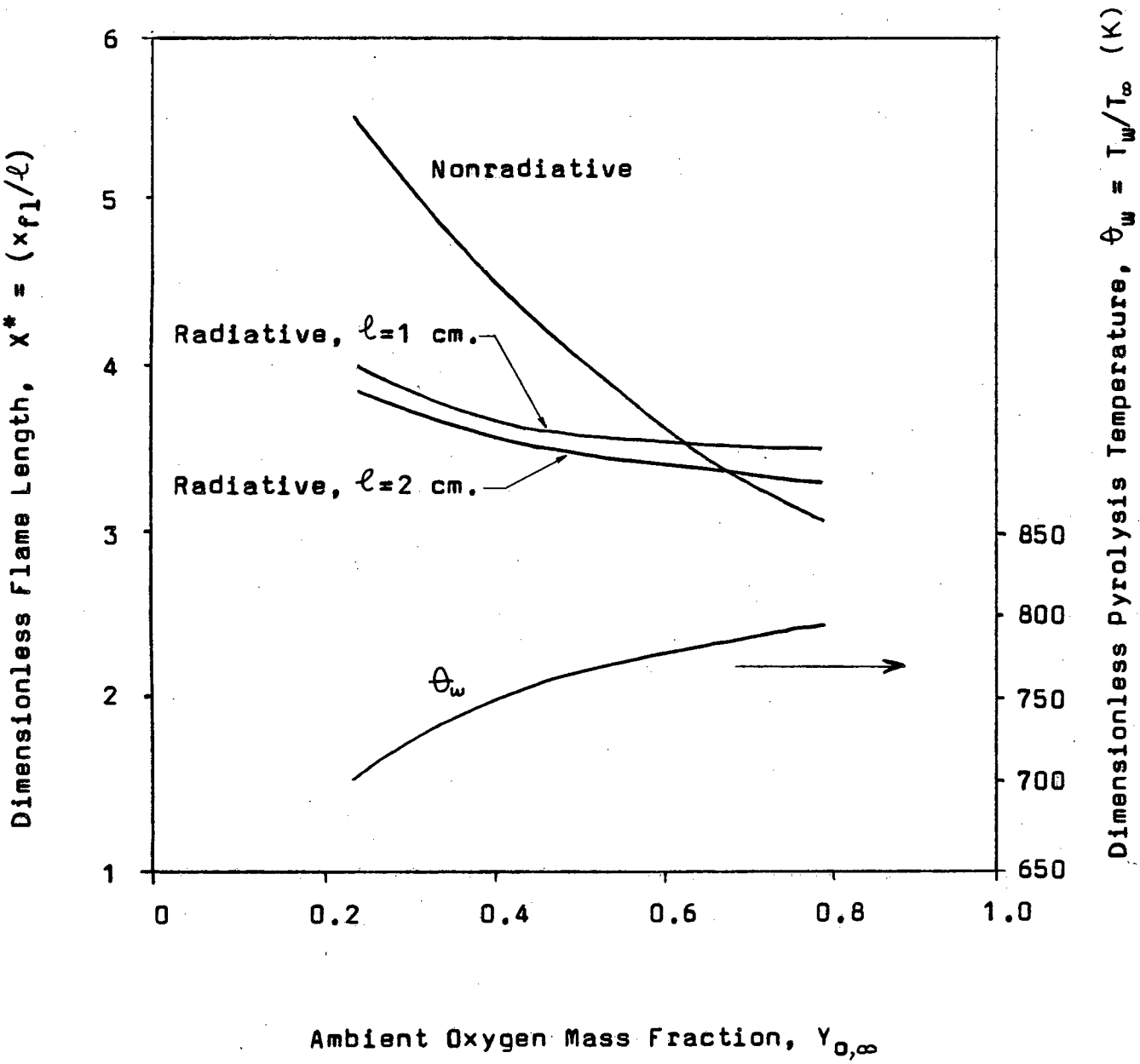
Nonradiative
Radiative, ℓ=1 cm.
Radiative, ℓ=2 cm.
θ_w
Dimensionless Flame Length, $X^* = (x_{f1}/\ell)$
Dimensionless Pyrolysis Temperature, $\theta_w = T_w/T_\infty$ (K)
Ambient Oxygen Mass Fraction, $Y_{O,\infty}$
1
2
3
4
5
6
650
700
750
800
850
0
0.2
0.4
0.6
0.8
1.0

Figure 11

NOMENCLATURE

B	mass transfer number, $(Q_p Y_{o,\infty} - h_w)/L$
c_p	mixture specific heat
D	diffusion coefficient
D_c	dimensionless heat of combustion, $Q_p Y_{o,\infty}/h_w$
e_b	black body emissive power , σT^4
f	similarity stream function in boundary layer
f_v	soot volume fraction
g	gravitational acceleration
Gr_x	Grashof number. $g(T_w - T_\infty)x^3/\nu_\infty^2 T_\infty$
h	enthalpy
k	thermal conductivity
L	latent heat of pyrolysis
$\dot{m}_p$	local mass flux
M	molecular weight
M_p	total mass flux
$\dot{m}'''$	volumetric mass generation rate
N_1	soot parameter, $K k_\infty/\sigma T_\infty^3$
N_2	length parameter, $2^{1/2}\sigma T_\infty^3 \ell / k_\infty Gr_\ell^{1/4}$
Pr	Prandtl number, ν/α
$\dot{q}'''$	Volumetric heat generation rate
q	heat flux
Q_r	dimensionless radiation flux, $q_r/\sigma T_\infty^4$
Q_p	heat of reaction per gram of oxygen
r	mass consumption number, $Y_o \nu_f M_f / Y_{fw} \nu_o M_o$

T	temperature
u	x-direction velocity
v	y-direction velocity
x	streamwise coordinate
y	transverse coordinate
Y_i	mass fraction of species i

Greek

β	fuel-oxygen Shvab-Zeldovich variable, $(Y_f/\nu_f M_f)-(Y_o/\nu_o M_o)$
γ	enthalpy-oxygen Shvab-Zeldovich variable, $(h/Q)-(Y_o/\nu_o M_o)$
η	transformation coordinate
θ	dimensionless temperature, T/T_∞
κ	absorption coefficient
μ	viscosity
ν	stoichiometric coefficient or kinematic viscosity
ξ	transformation coordinate
ρ	density
τ	optical thickness, κy
ψ	stream function

Subscripts

c	conduction
e	excess
ex	external
f	fuel

fl	flame
o	oxygen
p	pyrolyzed
r	radiation
w	wall
w_o	value at wall without radiation
δ	boundary layer edge
∞	ambient

APPENDIX

The stagnant film problem is modeled as a one-dimensional film between two infinite screens. Beyond the screen at x=0 is a stagnant oxidizing gaseous ambiance, while beyond the screen at $x=x_w$ is a solid or liquid fuel reservoir. Combustion occurs within the film and is assumed to be steady and laminar. A constant mass flux, $\dot{m}=\rho v$ is assumed ρD is taken as a constant, the Lewis number is defined as α/D and radiation is neglected.

High molecular weight fuels diffuse more slowly than lighter fuels, resulting in Lewis numbers greater than one. Because many common fuels are heavy, the non-unity Lewis number problem is of great importance in the field of combustion.

The species and energy equations describing the system are

$$\frac{d^2 J_\beta}{d\xi} + Le_o \frac{dJ_\beta}{d\xi} = 0$$

$$\frac{d^2 J_\gamma}{d\xi^2} + \lambda \frac{dJ_\gamma}{d\xi} = 0$$

$$\frac{d^2 J_\gamma}{d\xi^2} + \frac{d}{d\xi}\left[J_\gamma - \frac{(Le_o-1)(1+r^{-1})}{(1-D_c^{-1})}\right] J_\beta = 0$$

where J_γ and J_β are the normalized Shvab-Zeldovich variables defined as

$$J_\gamma = \frac{-h/Q_p + (Y_{o,\infty}-Y_o)/\nu_o M_o}{-h_w/Q_p + Y_{o,\infty}/\nu_o M_o}$$

$$J_\beta = \frac{Y_f/\nu_f M_f + (Y_{o,\infty} - Y_o)/\nu_o M_o}{Y_{fw_o}/\nu_f M_f + Y_{o,\infty}/\nu_o M_o}$$

and ξ and λ are defined as

$$\xi = \frac{\dot{m}x}{\rho D Le_o} \qquad \text{and} \qquad \lambda = \frac{Le_o}{Le_f}$$

The boundary conditions are

$$x = 0, \quad J_\gamma = 0, \; J_\beta = 0$$

$$x = x_{fl}, \quad J_{\gamma_{fl}} = \frac{D_c - (h_{fl}/h_w)}{D_c - 1}, \quad J_{\beta_{fl}} = \frac{r}{r+1}$$

$$x = x_w, \quad J_{\gamma_w} \simeq 1, \; J_{\beta_w} = \frac{(Y_{fw}/Y_{fw_o}) + r}{r+1},$$

$$\left.\frac{dJ_\gamma}{d\xi}\right)_w = \frac{1}{B}\frac{(r+1)\,Y_{fw_o}}{Y_{ft} - Y_{fw}}\left.\frac{dJ_\beta}{d\xi}\right)_w$$

Solving the equations and boundary conditions yields expressions for ξ, J_γ, J_β, and the enthalpy, oxygen and fuel ratios

$$\xi = \begin{cases} \dfrac{1}{Le_o}\ln\left[\dfrac{(r+1)(B+1)}{1+B+r}\right], & x = x_{fl} \\[2ex] \dfrac{1}{\lambda}\ln\left[\dfrac{e^{-\xi_{fl}}}{\lambda e^{-\lambda\xi_{fl}}}\left\{1 + B\left[1 + \dfrac{1/Le_o - (e^{\xi_{fl}/Le_o} - 1)/(e^{\xi_{fl}} - 1)}{(1 - D_c^{-1})}\right]\right\}\right], & x = x_w \end{cases}$$

$$J_\gamma = \begin{cases} \left(\dfrac{1-e^{-\xi}}{1-e^{-\xi_{fl}}}\right)\left[J_{\gamma_{fl}} + \dfrac{1}{Le_o(1-D_c^{-1})}\right] - \left(\dfrac{1-e^{-Le_o\xi}}{1-e^{-Le_o\xi_{fl}}}\right)\dfrac{1}{Le_o(1-D_c^{-1})} & , 0 \le x \le x_{fl} \\ 1 + \left(\dfrac{e^{-\lambda\xi} - e^{-\lambda\xi_w}}{e^{-\lambda\xi_{fl}} - e^{-\lambda\xi_w}}\right)(J_{\gamma_{fl}} - 1) & , x_{fl} \le x \le x_w \end{cases}$$

where $J_{\gamma fl} = 1 - \dfrac{\exp(\lambda\xi_w - \lambda\xi_{fl}) - 1}{B}$

$$J_\beta = (1 + B^{-1})(1 - e^{-Le_o\xi})$$

$$\frac{h}{h_w} = \begin{cases} D_c(1+r^{-1})J_\beta - (D_c - 1)J_\gamma & , 0 \le x \le x_{fl} \\ D_c - (D_c - 1)J_\gamma & , x_{fl} \le x \le x_w \end{cases}$$

$$\frac{Y_o}{Y_{o,\infty}} = \begin{cases} 1 - (1+r^{-1})J_\beta & , 0 \le x \le x_{fl} \\ 0 & , x_{fl} \le x \le x_w \end{cases}$$

$$\frac{Y_f}{Y_{fw}} = \begin{cases} 0 & , 0 \le x \le x_{fl} \\ (1+r)J_\beta - r & , x_{fl} \le x \le x_w \end{cases}$$

The equations and boundary conditions have been solved for a solid fuel polymethylmethacrylate (PMMA), with the following properties

r = Mass consumption number = 0.2

B = Mass transfer number = 1.5

D_c = Dimensionless heat of combustion = 5.0

θ_w = Dimensionless pyrolysis temperature = 2.5

The properties of air were taken as

P = 1 atm.

T = 298 K

ρD = 3.0 x 10 kg/ms

c_p = 1.3 kJ/kgK

$Y_{o,\infty}$ = 0.23

Pr = 0.73

and x_w was taken as 0.01 m in all cases.

Initially the fuel Lewis number, Le_f, and the oxidant Lewis number, Le_o, were assumed equal. J_γ, J_β, Y_f, Y_o and T profiles are plotted for the Lewis number varying from 0.5 to 5.0 in Figures 1A through 4A .

The fuel and oxidant Lewis numbers were then varied independently, with Le_f=1.0 while Le_o was varied and Le_o=1.0 while Le_f was varied. $J_{\gamma fl}$, $J_{\beta w}$, ξ_w, $\dot{m}'''$, Y_{fw}, T_{fl} and x_{fl} are shown plotted against the Lewis number for both the $Le_f = Le_o$ and the $Le_f \neq Le_o$ cases in Figures 5A-11A .

The Lewis number is defined as the ratio of energy diffusion to mass diffusion. A high Lewis number indicates more energy transfer. This is verified in the $Le_f \neq Le_o$ results. Because the flame is closer to the fuel side, increasing Le_f has a greater effect than

increasing Le_o. Increasing Le_f allows more energy to reach the fuel, while increasing Le_o allows more energy to diffuse towards the oxidant. These effects are verified by the results shown in Figures 5A-11A and are consistent with the results reported by Kassoy and Williams [7].

APPENDIX FIGURE CAPTIONS

1A The normalized enthalpy-oxygen variable, J_γ, vs. the dimensionless distance for PMMA. The Lewis number is varied from 0.5 to 5.0, where $Le_o=Le_f=Le$.

2A The normalized fuel-oxygen variable, J_β, vs. the dimensionless distance for PMMA. The Lewis number is varied from 0.5 to 5.0, where $Le_o=Le_f=Le$.

3A The fuel mass fraction, represented by the solid curve, and the oxygen mass fraction. represented by the dashed curve, vs. the dimensionless distance for PMMA. The Lewis number is varied from 0.5 to 5.0, where $Le_o=Le_f=Le$

4A The temperature vs. the dimensionless distance for PMMA. The Lewis number is varied from 0.5 to 5.0, where $Le_o=Le_f=Le$.

5A $J_{\gamma fl}$ vs. Le_o, Le_f and Le for PMMA where $Le=Le_o=Le_f$. $Le_f=1.0$ when Le_o is varied; $Le_o=1.0$ when Le_f is varied.

6A $J_{\beta w}$ vs. Le_o, Le_f and Le for PMMA, where $Le=Le_o=Le_f$. $Le_f=1.0$ when Le_o is varied; $Le_o=1.0$ when Le_f is varied.

7A Dimensionless mass flux vs. Le_o, Le_f and Le for PMMA, where $Le=Le_o=Le_f$. $Le_f=1.0$ when Le_o is varied; $Le_o=1.0$ when Le_f is varied.

8A Mass flux vs. Le_o, Le_f and Le for PMMA where $Le=Le_o=Le_f$. $Le_f=1.0$ when Le_o is varied; $Le_o=1.0$ when Le_f is varied.

9A Wall fuel mass fraction vs. Le_o, Le_f and Le for PMMA, where $Le=Le_o=Le_f$. $Le_f=1.0$ when Le_o is varied; $Le_f=1.0$ when Le_o is varied.

10A Flame temperature vs. Le_o, Le_f and Le for PMMA, where $Le=Le_o=Le_f$. $Le_f=1.0$ when Le_o is varied; $Le_o=1.0$ when Le_f is varied.

11A Flame location vs. Le_o, Le_f and Le for PMMA where $Le=Le_o=Le_f$. $Le_f=1.0$ when Le_o is varied; $Le_o=1.0$ when Le_f is varied.

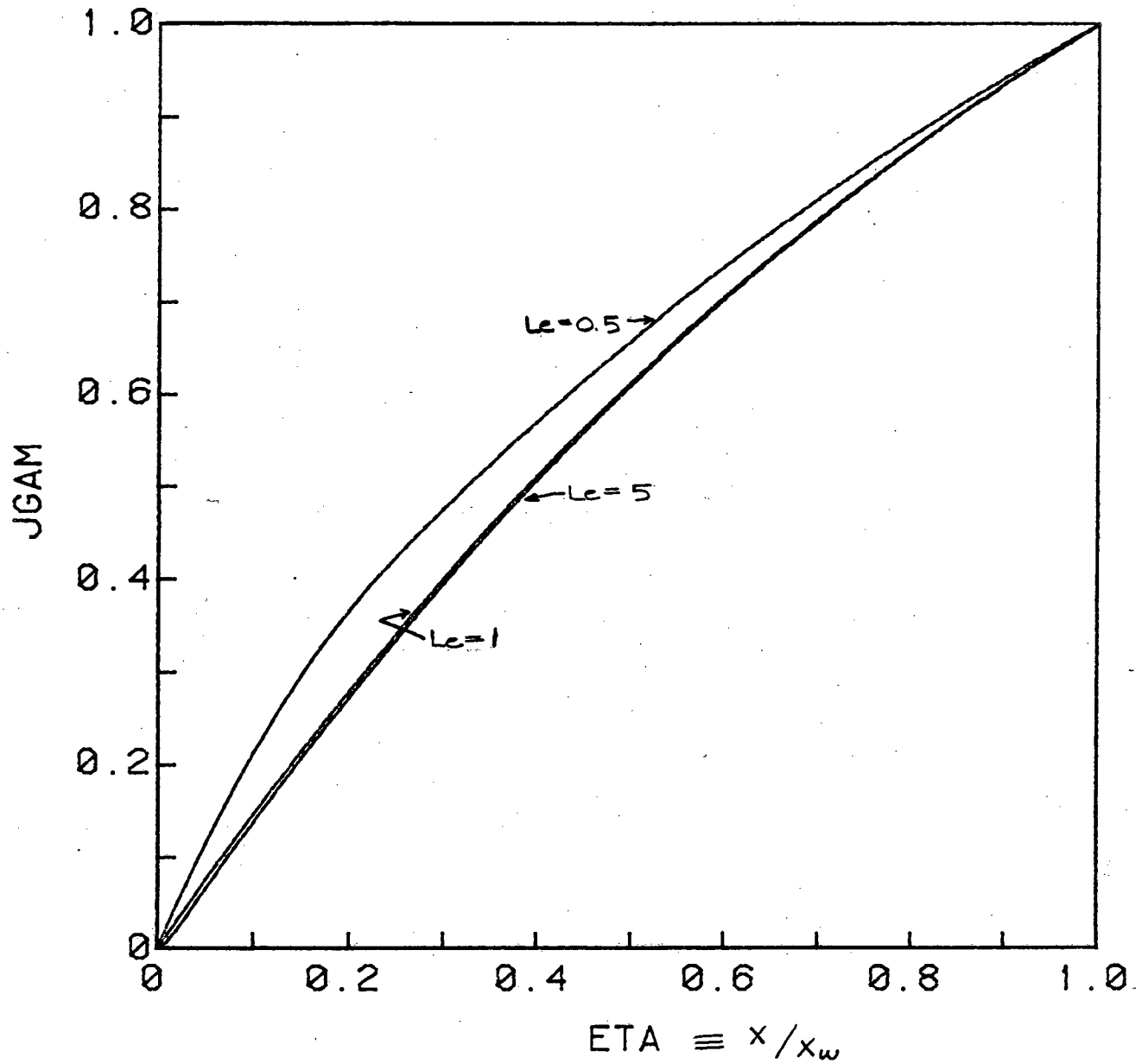

Figure 1A

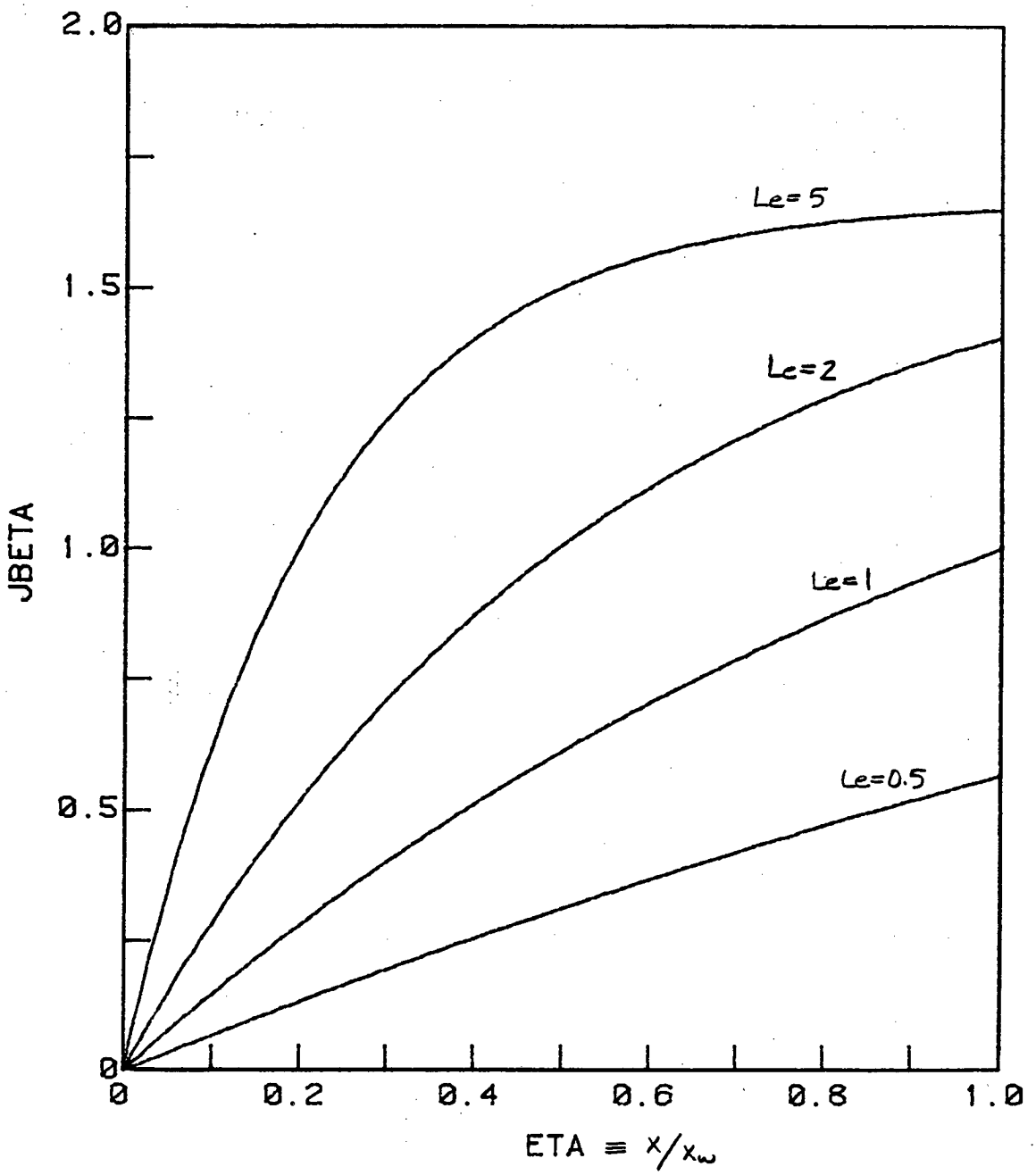

Figure 2A

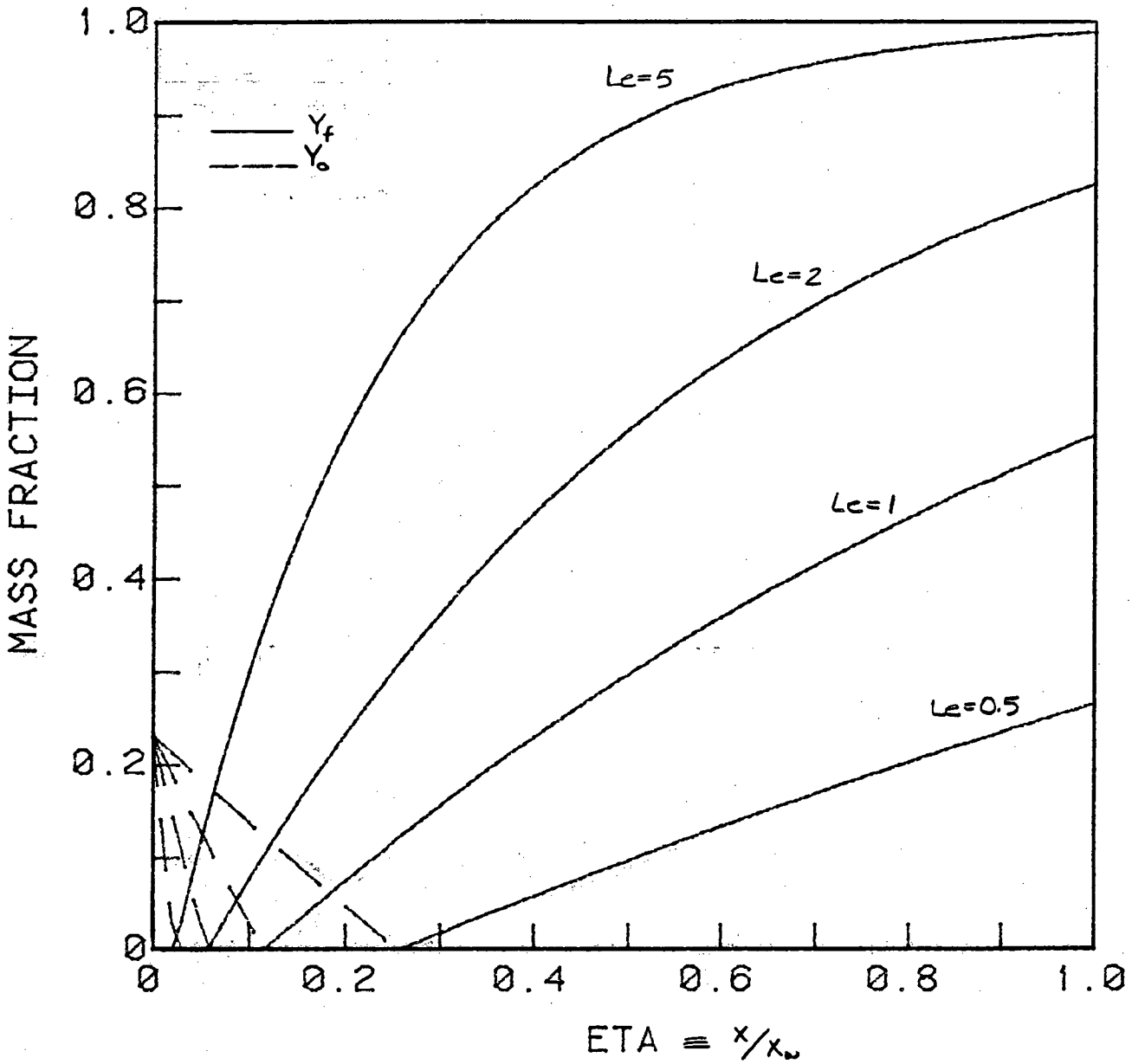
1.0
0.8
0.6
0.4
0.2
0
MASS FRACTION
Y_f
Y_o
Le=5
Le=2
Le=1
Le=0.5
0
0.2
0.4
0.6
0.8
1.0
ETA ≡ x/x_w

Figure 3A

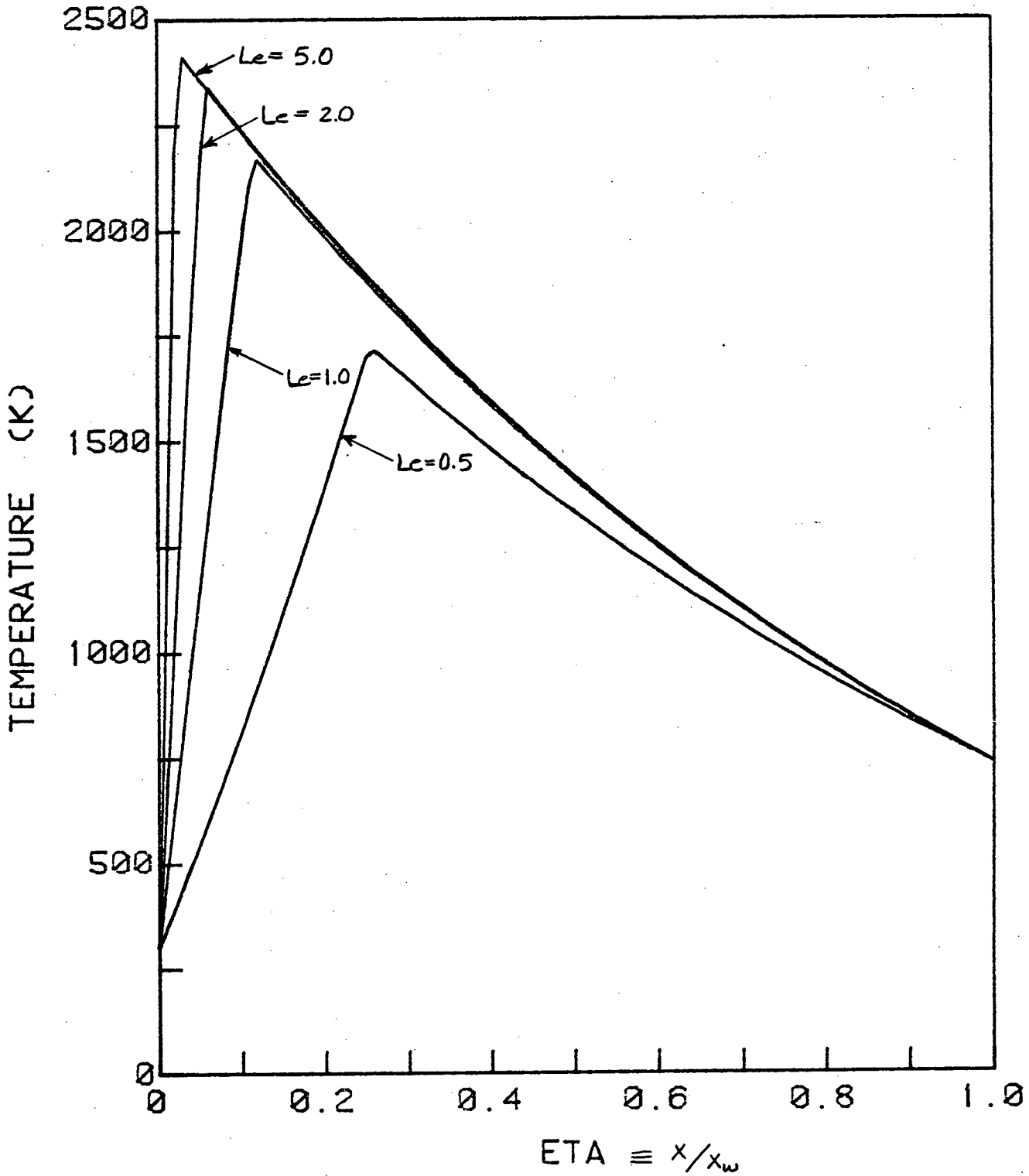
2500
2000
1500
1000
500
0
TEMPERATURE (K)
Le= 5.0
Le= 2.0
Le=1.0
Le=0.5
0
0.2
0.4
0.6
0.8
1.0
ETA ≡ x/xw

Figure 4A

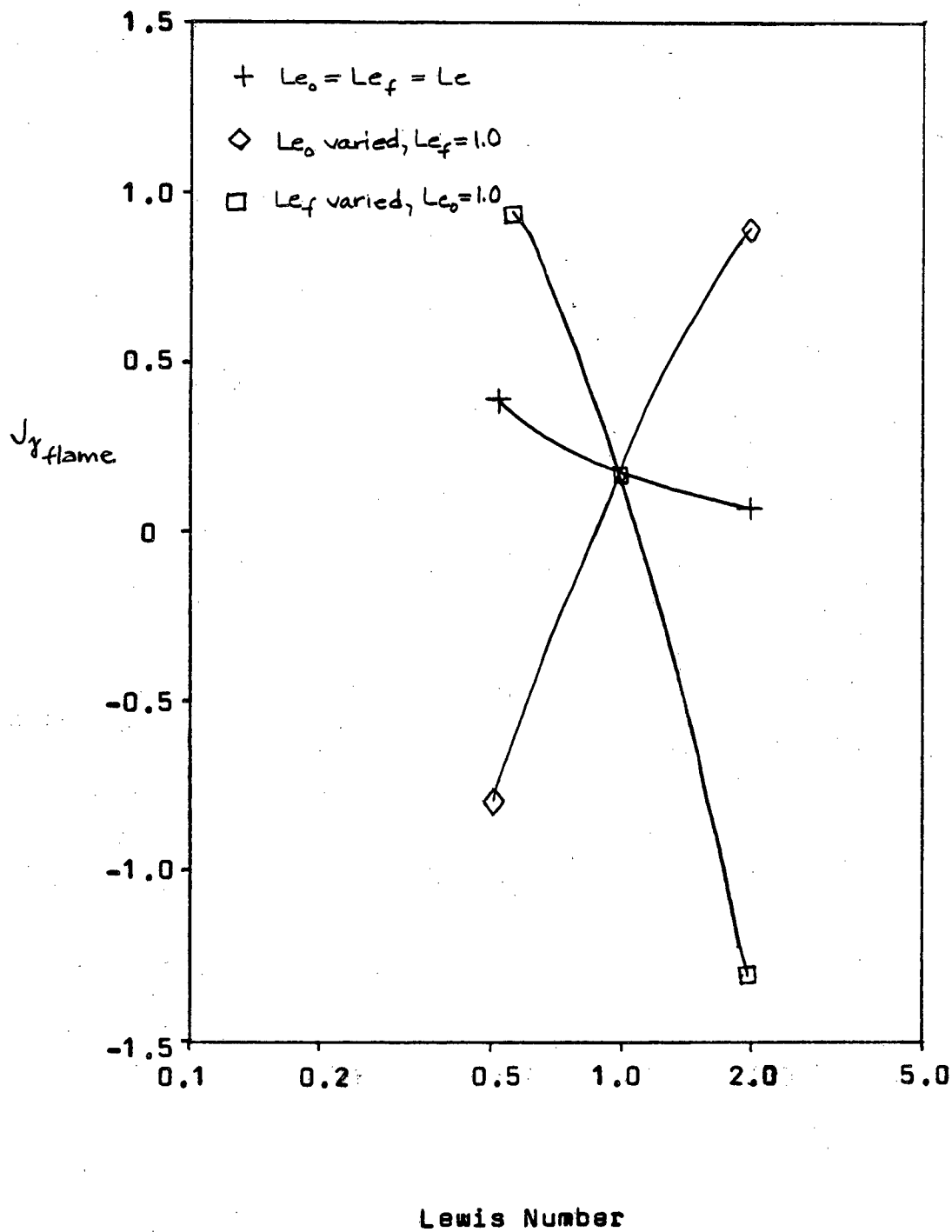
1.5
1.0
0.5
0
-0.5
-1.0
-1.5
$J_{\gamma_{flame}}$
+ $Le_o = Le_f = Le$
◇ Le_o varied, $Le_f = 1.0$
□ Le_f varied, $Le_o = 1.0$
0.1
0.2
0.5
1.0
2.0
5.0
Lewis Number

Figure 5A

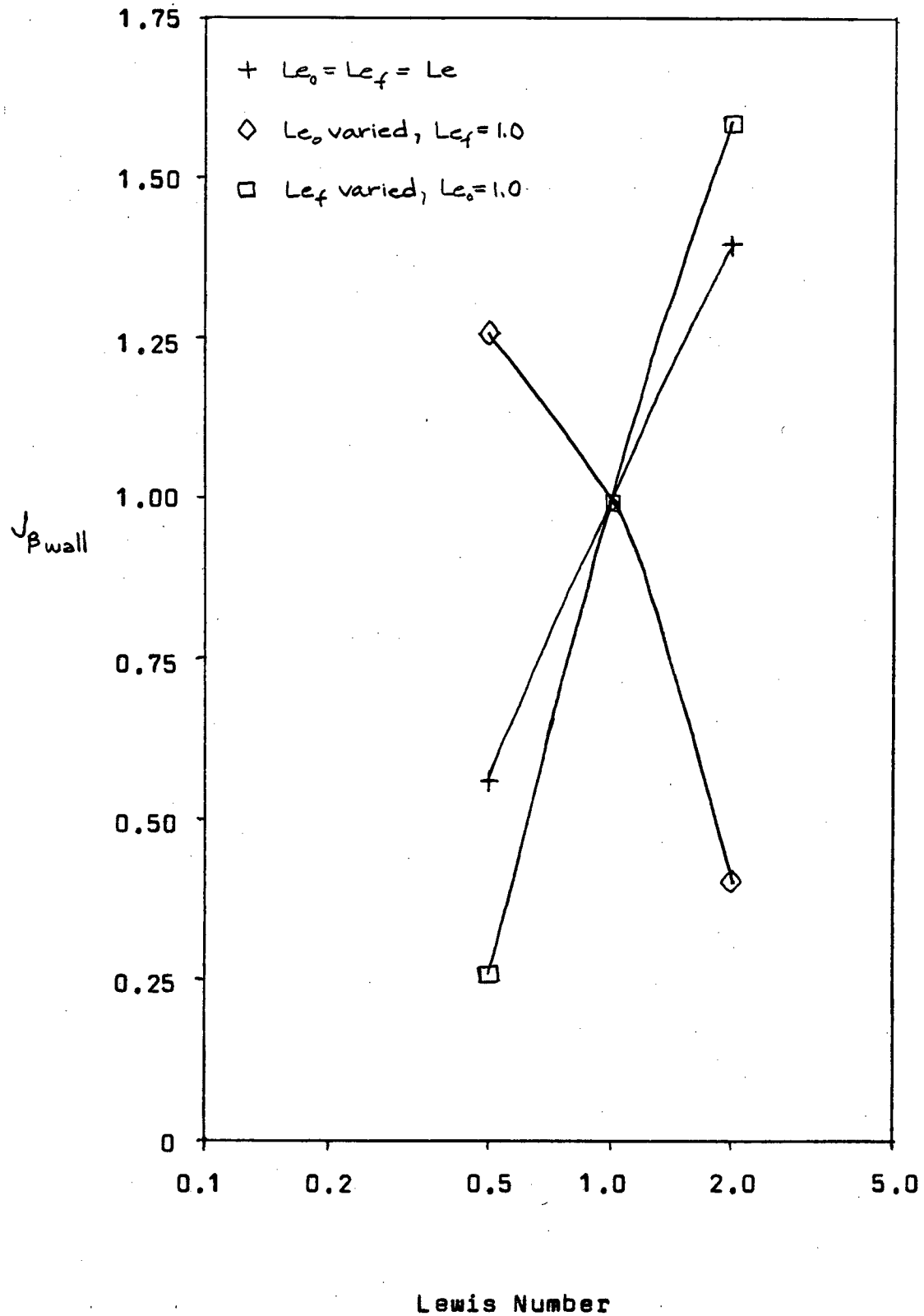
1.75
1.50
1.25
1.00
0.75
0.50
0.25
0
$J_{\beta wall}$
+ $Le_o = Le_f = Le$
◇ Le_o varied, $Le_f = 1.0$
□ Le_f varied, $Le_o = 1.0$
0.1
0.2
0.5
1.0
2.0
5.0
Lewis Number

Figure 6A

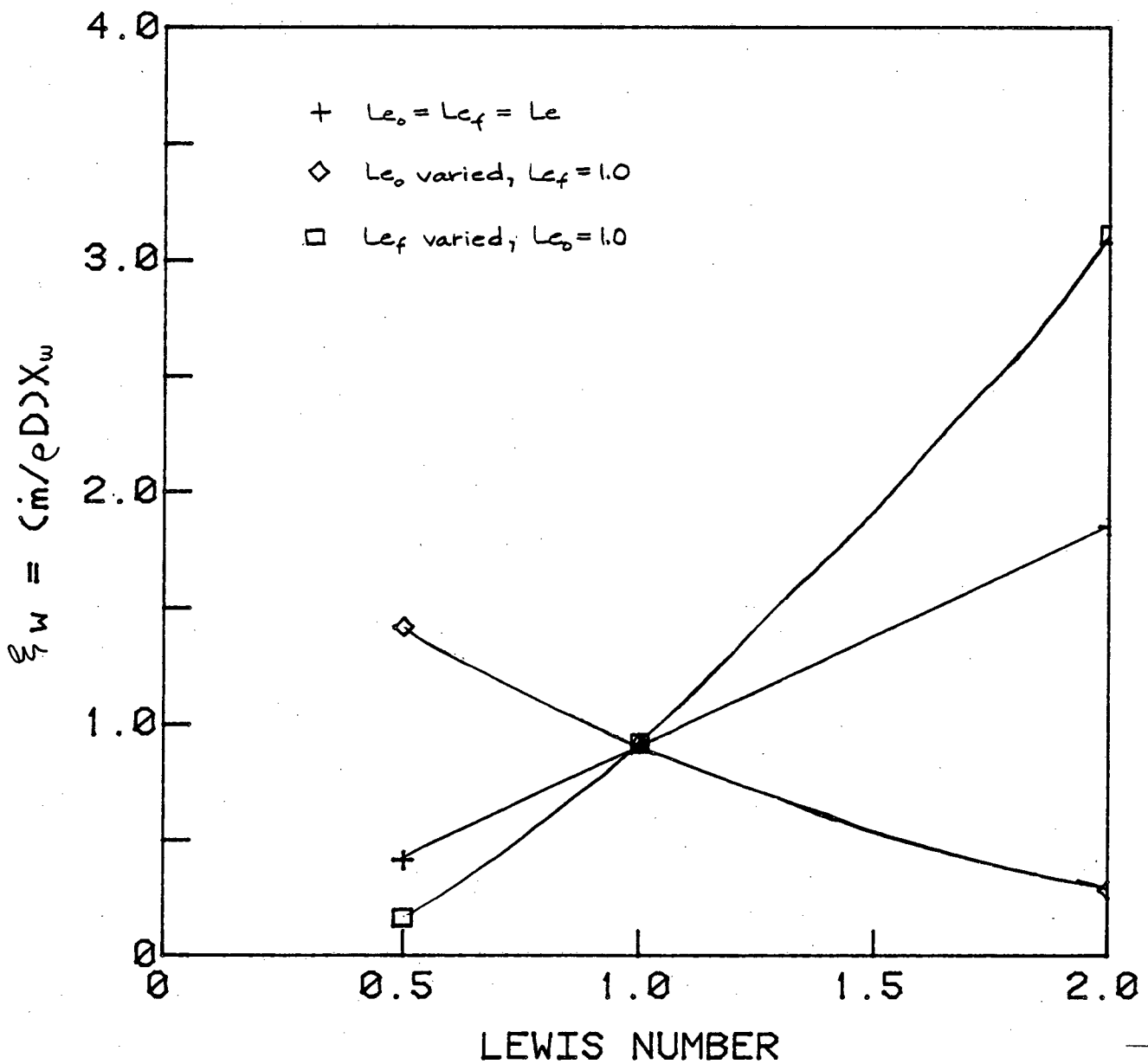
4.0
3.0
2.0
1.0
0
0
0.5
1.0
1.5
2.0
LEWIS NUMBER
$\xi_w = (\dot{m}/\rho D)X_w$
+ $Le_o = Le_f = Le$
◇ Le_o varied, $Le_f = 1.0$
□ Le_f varied, $Le_o = 1.0$

Figure 7A

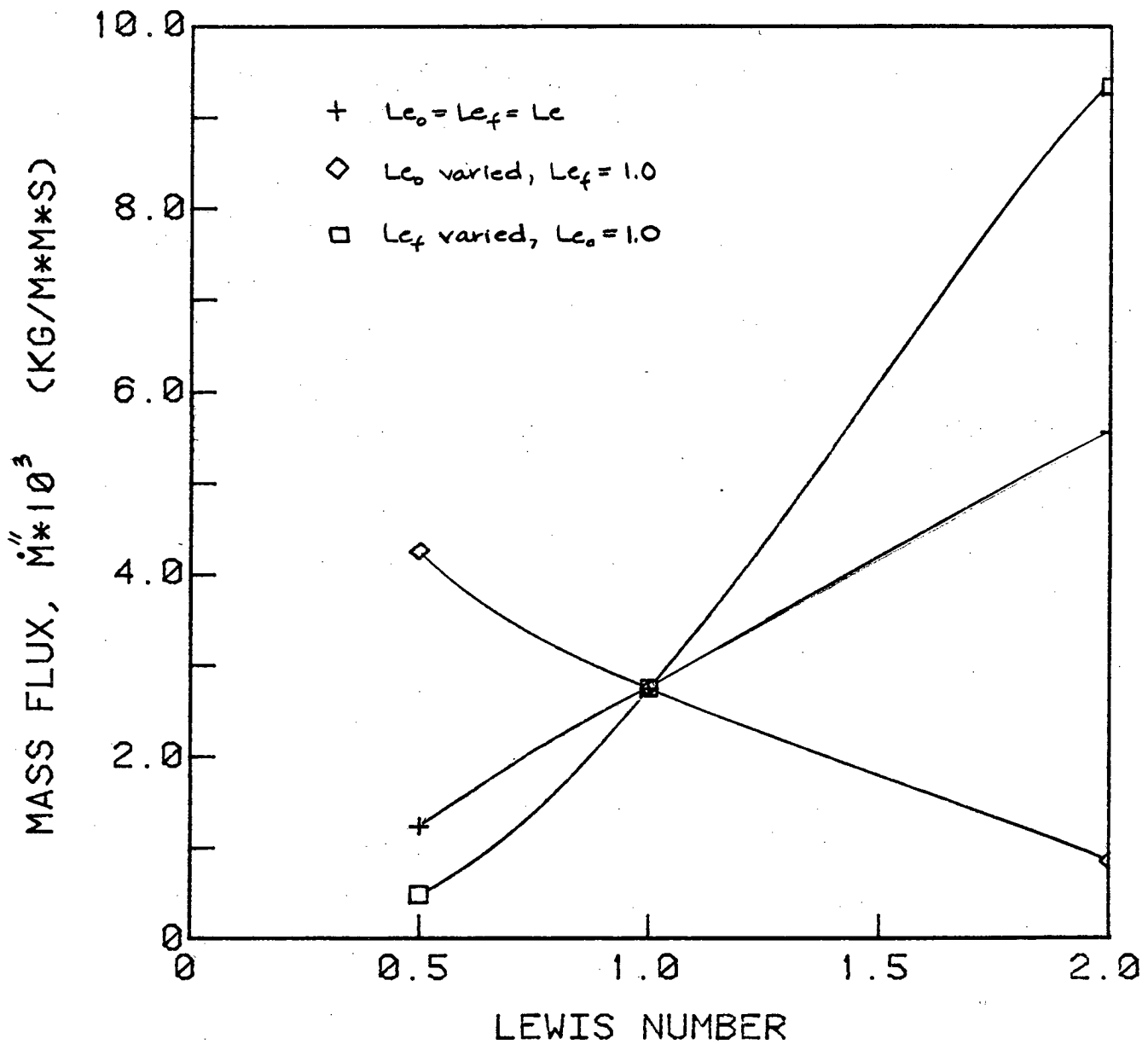
10.0
8.0
6.0
4.0
2.0
0
0
0.5
1.0
1.5
2.0
MASS FLUX, $\dot{M}''*10^3$ (KG/M*M*S)
LEWIS NUMBER
+ $Le_o = Le_f = Le$
◇ Le_o varied, $Le_f = 1.0$
□ Le_f varied, $Le_o = 1.0$

Figure 8A

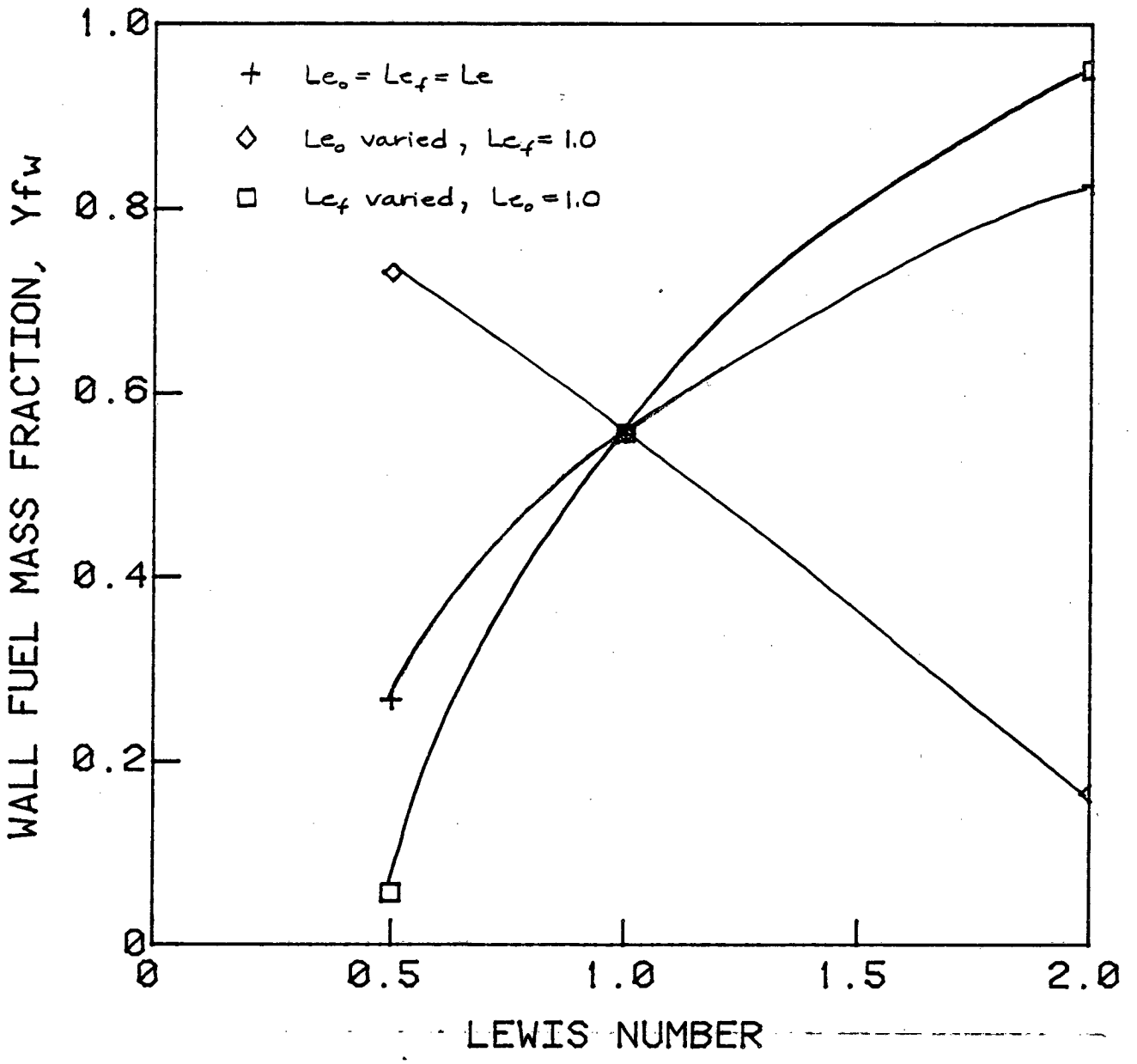
1.0
0.8
0.6
0.4
0.2
0
WALL FUEL MASS FRACTION, Yfw
+ Le₀ = Le_f = Le
◇ Le₀ varied, Le_f = 1.0
□ Le_f varied, Le₀ = 1.0
0
0.5
1.0
1.5
2.0
LEWIS NUMBER

Figure 9A

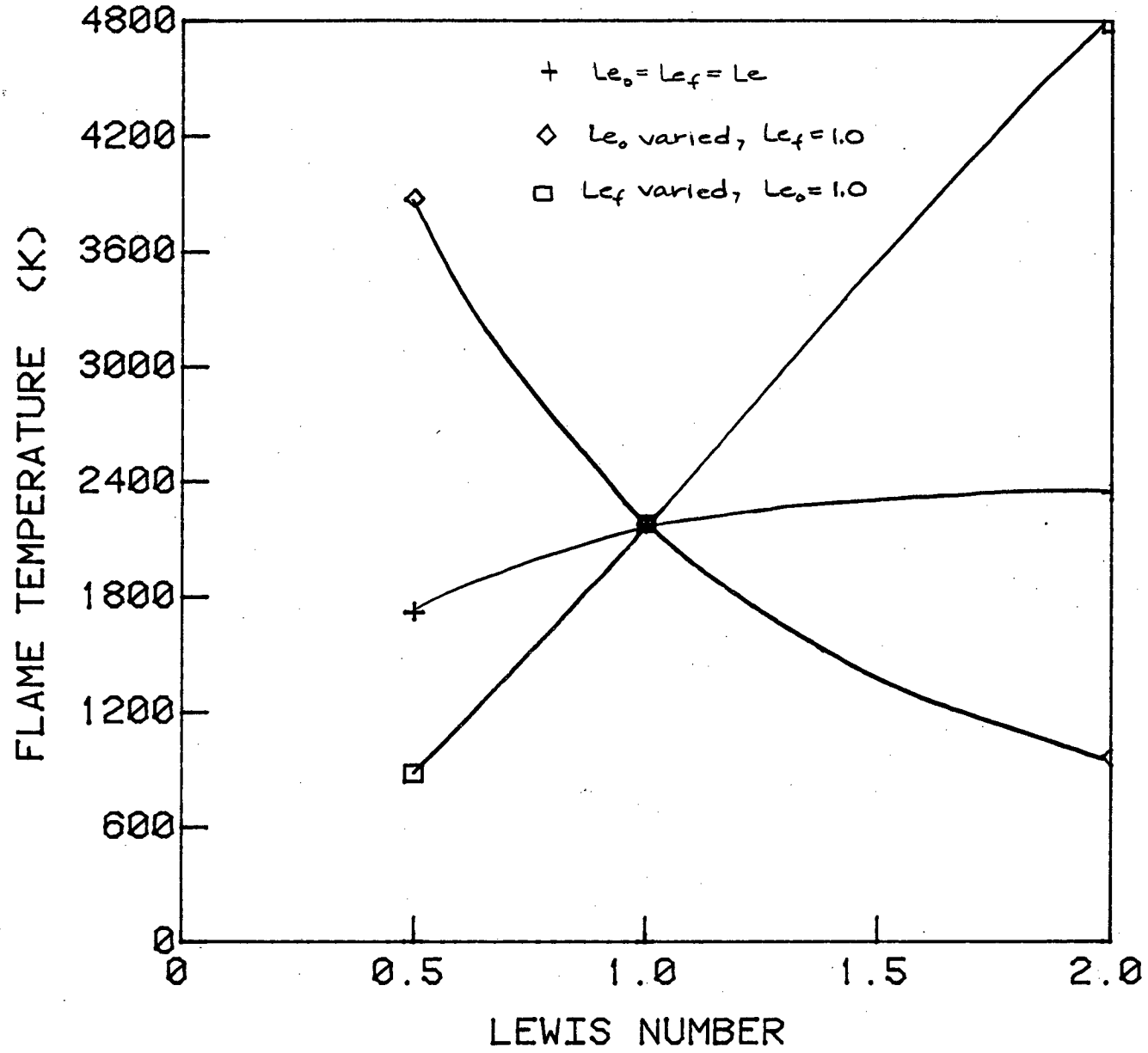
4800
4200
3600
3000
2400
1800
1200
600
0
FLAME TEMPERATURE (K)
0
0.5
1.0
1.5
2.0
LEWIS NUMBER
+ Le₀ = Le_f = Le
◇ Le₀ varied, Le_f = 1.0
□ Le_f varied, Le₀ = 1.0

Figure 10A

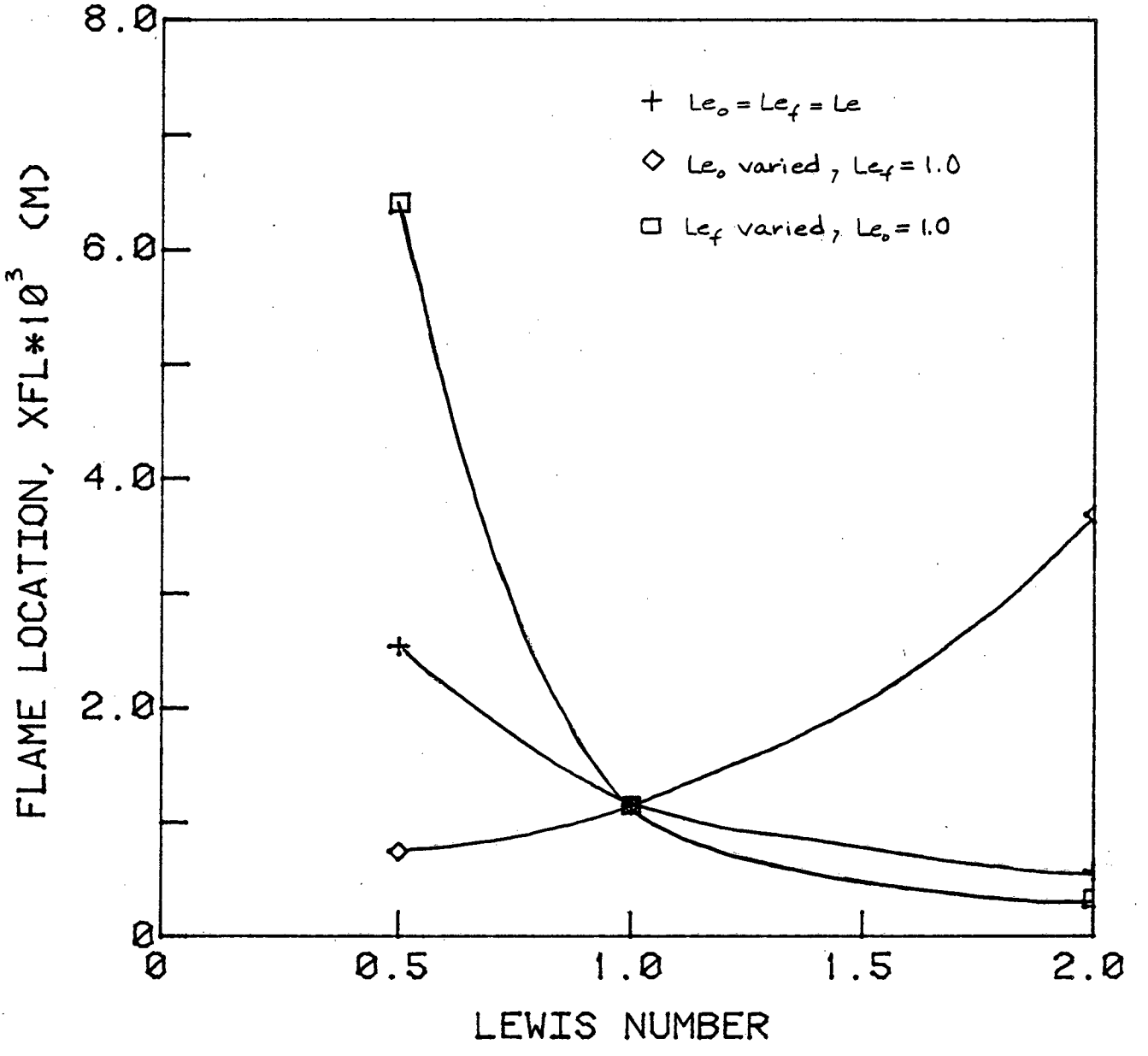
8.0
6.0
4.0
2.0
0
0
0.5
1.0
1.5
2.0
FLAME LOCATION, XFL*10^3 (M)
LEWIS NUMBER
+ Le_o = Le_f = Le
◇ Le_o varied, Le_f = 1.0
□ Le_f varied, Le_o = 1.0

Figure 11A

This report was done with support from the Department of Energy. Any conclusions or opinions expressed in this report represent solely those of the author(s) and not necessarily those of The Regents of the University of California, the Lawrence Berkeley Laboratory or the Department of Energy.

Reference to a company or product name does not imply approval or recommendation of the product by the University of California or the U.S. Department of Energy to the exclusion of others that may be suitable.

TECHNICAL INFORMATION DEPARTMENT
LAWRENCE BERKELEY LABORATORY
UNIVERSITY OF CALIFORNIA
BERKELEY, CALIFORNIA 94720